

**UNIVERSIDAD DE SANTIAGO DE CHILE**  
**FACULTAD DE CIENCIAS**  
**Departamento de Física**



**Langevin Dynamics for Gas Transport in Carbon Nanotubes**

**Gastón Antonio González Teruel**

**Profesor guía: Felipe Herrera**

**Tesis para optar al Grado académico de  
Magíster en Ciencia mención  
Física**

**Santiago – Chile**

**2021**

© Gastón Antonio González Teruel , 2021



• Algunos derechos reservados. Esta obra está bajo una Licencia Creative Commons Atribución-Chile 3.0. Sus condiciones de uso pueden ser revisadas en:  
<http://creativecommons.org/licenses/by/3.0/cl/>.

# **Langevin Dynamics approach for Gas Transport in Carbon Nanotubes**

**Gastón Antonio González Teruel**

Este trabajo de titulación fue elaborado bajo la supervisión del profesor Dr. Felipe Herrera Urbina del Departamento de Física y ha sido aprobado por los miembros de la comisión calificadora del candidato, Dr. , Dr. y Dr. .

Dr. \_\_\_\_\_

Dr. \_\_\_\_\_

Dr. \_\_\_\_\_

---

Dr.  
Director de Departamento

---

Dr. Felipe Herrera  
Profesor guía

## RESUMEN

En esta tesis, se estudia un algoritmo unidimensional de dinámica estocástica de Langevin implementado en MATLAB para calcular la auto-difusión de moléculas de nitrógeno diatómico dentro de un nanotubo de carbono de pared simple, de radio 4.3Å, en un rango de temperaturas entre 10K y 300K. El algoritmo de dinámica de Langevin introduce un parámetro de amortiguamiento  $\gamma$  que es posible de elegir convenientemente para capturar adecuadamente interacciones térmicas e interatómicas en el sistema. La molécula de nitrógeno se considera como una esfera sólida con la masa de nitrógeno diatómico. Se obtuvieron potenciales efectivos entre las interacciones carbono-nitrógeno molecular y las interacciones intermoleculares del nitrógeno. Se encontró que el potencial azimutal no es relevante para la difusión axial. Además, el potencial radial tiene dos mínimos que son las posiciones privilegiadas donde las moléculas de nitrógeno son capaces de difundir a lo largo del nanotubo. El potencial axial tiene una profundidad aproximada de 17K y tiene la periodicidad de la celda unitaria del nanotubo.

Para comparar la precisión de los resultados obtenidos con una propagación estocástica, se usó el programa de dinámica molecular 3D LAMMPS para obtener la difusión de una molécula de nitrógeno molecular a diferentes temperaturas dentro del nanotubo de carbono. Se buscó un parámetro  $\gamma$  de tal forma que los datos coincidieran. El parámetro  $\gamma$  que es consistente los datos obtenidos con LAMMPS corresponde al valor de 0.1 THz, donde se observaron diferencias por debajo 10K y por sobre los 300K. Se calcularon las difusiones a distintas concentraciones de nitrógeno con LAMMPS y con 1D Langevin, donde luego al compararlas se encontró que a bajas concentraciones las difusiones se encuentran en el mismo orden de magnitud, pero a altas concentraciones cercanas al punto de saturación del nanotubo, el algoritmo 1D Langevin subestima el coeficiente de difusión, que se puede explicar por la mayor disponibilidad de trayectorias axiales de difusión en 3D, en comparación con lo modelado 1D.

**Palabras Claves:** MATLAB, Nanotubo, Difusión, Dinamica Langevin, LAMMPS

## ABSTRACT

In this thesis, a one-dimensional Langevin stochastic dynamics algorithm implemented in MATLAB is studied to calculate the self-diffusion of diatomic nitrogen molecules within a single-walled carbon nanotube, of radius 4.3Å, in a temperature range between 10K and 300K. The Langevin dynamics algorithm introduces a damping parameter  $\gamma$  that can be conveniently chosen to adequately capture thermal and interatomic interactions in the system. The nitrogen molecule is considered as a solid sphere with the mass of diatomic nitrogen. Effective potentials were obtained between molecular carbon-nitrogen interactions and intermolecular nitrogen interactions. It was found that the azimuthal potential is not relevant for axial diffusion. Furthermore, the radial potential has two minima, which are the privileged positions where the nitrogen molecules are able to diffuse along the nanotube. The axial potential has a depth of approximately 17K and has the periodicity of the unit cell of the nanotube.

To compare the precision of the results obtained with a stochastic propagation, the 3D molecular dynamics program LAMMPS was used to obtain the diffusion of a molecule of molecular nitrogen at different temperatures within the carbon nanotube. A parameter  $\gamma$  was searched in such a way that the data matched. The parameter  $\gamma$  that is consistent with the data obtained with LAMMPS corresponds to the value of 0.1 THz, where differences were observed below 10K and above 300K. Diffusions at different nitrogen concentrations were calculated with LAMMPS and 1D Lagenvin, where after comparing them it was found that at low concentrations the diffusions are in the same order of magnitude, but at high concentrations close to the saturation point of the nanotube, the 1D Langevin algorithm underestimates the diffusion coefficient, which can be explained by the greater availability of axial diffusion paths in 3D, compared to 1D modeling.

**Keywords:** MATLAB, Nanotube, Self-Diffusion, Langevin Dynamics, LAMMPS

# CONTENTS

<b>1 Gas Transport in Porous Media and Langevin Dynamics</b>	<b>1</b>
1.1 Nanotubes . . . . .	2
1.2 Molecular Sieving in Nanotubes . . . . .	4
1.3 Langevin Transport Dynamics . . . . .	6
1.4 Diffusion Coefficient from Stochastic Dynamics . . . . .	8
<b>2 Computational Langevin Dynamics</b>	<b>11</b>
2.1 Stochastic Molecular Dynamics Algorithm . . . . .	12
2.1.1 Verlet leap frog algorithm . . . . .	13
2.1.2 Impulsive Langevin Leap-Frog algorithm . . . . .	14
2.1.3 Flying Ice cube effect . . . . .	17
2.1.4 Lennard-Jones Potential . . . . .	17
<b>3 Nitrogen Diffusion in Carbon Nanotubes</b>	<b>19</b>
3.1 Nitrogen-Nanotube Interaction Potential . . . . .	20
3.2 Intermolecular Potential . . . . .	23
3.3 Single Molecule Diffusion . . . . .	24
3.4 Density-Dependent Diffusion . . . . .	26
3.5 Future Work . . . . .	29
<b>4 CONCLUSIONS</b>	<b>31</b>
<b>Referencias bibliográficas</b>	<b>32</b>
<b>Anexos</b>	<b>35</b>
<b>A Description of the MATLAB Langevin Program</b>	<b>35</b>
<b>B Lammps Input Script</b>	<b>37</b>

## LIST OF TABLES

1.1 Classes of microporous materials and their properties adapted from Cundy & Cox (2005), Stock & Biswas (2012), Saufi & Ismail (2004) . . . . .	2
3.1 $C - N$ and $N - N$ Lennard-Jones interaction parameters taken from Arora & Sandler (2006),Bojan & Steele (1987). . . . .	20
3.2 $C - N_2$ and $N_2-N_2$ Lennard-Jones interaction parameters at T=100K . . . . .	24

# LIST OF FIGURES

1.1	Example of microporous materials in new technological uses. Carbon capture. Water desalination and energy storage. Microporous membrane components include zeolites, MOFs, carbon nanotubes, organic nanotubes, and inherently microporous polymers. Adapted from Li et al. (2018) . . . . .	2
1.2	Rolling of a single layer sheet into a nanotube. Taken from Aqel et al. (2012) . . . . .	3
1.3	(a) Schematic structure of a sheet. Nanotubes can be formed by folding the sheet along lattice vectors. The two basis vectors $a_1$ and $a_2$ are shown. Folding of the (8,8), (8,0), and (10,-2) vectors lead to armchair (b), zigzag (c), and chiral (d) tubes, respectively. Adapted from Dai (2002) . . . . .	4
1.4	Simplified diagram of molecular separation. Taken from Khataee et al. (2017) . . . . .	5
1.5	Simplified diagram of molecular transport. Effects of adsorption, transport in the pore, diffusion and bulk solution transport. Adapted from Moon (2019) . . . . .	6
2.1	Simplified diagrams of the problem . . . . .	11
2.2	(a) Radial potential SWCNT (15,0), (b) Mean square displacements for nitrogen in SWCNs on a log-log plot, (c) Loading vs pressure SWCNT (15,0), (d) Nitrogen self-Diffusion in SWCN as a function of load. Figure taken from Arora et al. (2004)	12
2.3	Diffusion and pressure, where a phase transition is observed at 100K. Taken from Sokhan et al. (2004) . . . . .	13
2.4	Plot of the Lennard-Jones potential function: Intermolecular potential energy as a function of the distance of a pair of particles. . . . .	18
3.1	Three-dimensional model of the carbon nanotube used. (15,0) . . . . .	19
3.2	Representation of the orientations that nitrogen can adopt. For each configuration, different potentials are obtained as a function of their distances from their respective centers of mass. . . . .	20
3.3	Potential $C - N_2$ in Kelvin. (a) Potentials as a function of the distance between Carbon and the center of mass of $N_2$ . Each curve (5000) is a potential with random orientations of $N_2$ . (b) Blue. Potential as a function of the distance between Carbon and Nitrogen according to table 3.1. Red. Potential as a function of distance at 100K weighted with the equation (3.1) of 5000 possible orientations. (c) Blue. Potential as a function of the radius between Carbon and Nitrogen according to table 3.1. Red. Potential as a function of radius with the potential calculated in the previous Figure 3.3 . . . . .	21
3.4	$N_2 - C$ Potential energy in Kelvin of the Zig Zag nanotube (15,0) with radius of 5.87Å. (a) Axial Potential within the nanotube. (b) Representation Radial-Azimuthal potential. (c) Magnification in a small region of the nanotube, around the minimum of the axial potential. . . . .	22
3.5	$N_2 - C$ Axial Potential energy in Kelvin. (a) Blue: Axial potential of an isolated nanotube. Black: Limitation of where the nanotube would be found. (b) Blue: Axial potential along the minimum in the nanotube. Inset: Close up of the image of the potential with a periodicity of 2.15Å between minima. . . . .	23
3.6	$N_2 - N_2$ Potential energy in Kelvin. (a) Potentials as a function of the distance between $N_2 - N_2$ , each curve (5000) is a potential with random orientations. (b) Potential as a function of the distance between $N_2 - N_2$ at different temperatures .	24
3.7	(a) Diffusion vs Temperature. Yellow: Theoretical free particle diffusion (1) as a function of temperature with $\gamma = 0.1$ THz. Black: 3D simulated diffusion MD one-particle (1) as a function of temperature. Blue: 1D Langevin simulated diffusion one-particle as a function of temperature. (b) $1/T$ Vs $\ln(D)$ of the diffusion obtained with our program and those of the lamps and their respective linear fitting, where the slope corresponds to the activation energy (K) according to eq.1.12 . . . . .	25

3.8	(a) Position vs time 5 Particles, calculated with 1D Langevin at T=100K, $\gamma = 0.1$ THz, 1ns. (b) Velocity autocorrelation function for multiple number of particles in 1D Langevin . . . . .	26
3.9	Axial and radial spatial distribution of 50 nitrogen molecules inside the swcnt (15,0) at 100K calculated with LAMMPS and represented graphically with VMD (Humphrey et al., 1996) . . . . .	26
3.10	(a) Positions vs time 30 nitrogen molecules within SWCNT (15,0) obtained with 1D Langevin.(b) Velocity Vs Time of the center of mass of the 30 nitrogen molecules. (c) Importance of considering the ice cube effect at 100K, $\gamma = 0.1$ THz, 1D Langevin Blue: Diffusion and number of particles omitting Flying ice cube Effect correction Red: Diffusion vs number of particles considering the Flying ice cube Effect correction . . . . .	27
3.11	Diffusion Vs saturation point. Blue: MD LAMMPS, Red: 1D Langevin, Purple: Data reported by Sandler and Yellow: Free particle limit . . . . .	28
3.12	Characteristics of Nanotubes of different radius 8.6Å (22,0), 7.1Å (18,0), 5.87Å (15,0), 4.3Å (11,0). (a) Radial potential in Kelvin, (b) Axial potential in Kelvin, (c) representation of the radius of the Nanotubes. . . . .	29
3.13	(a) and (b) State of a Nanotube after 5ns in a medium in the presence of nitrogen molecules. (c) A $2 \times 1 \times 1$ supercell of the IZA structure framework of PSI (blue = Si and red = O atoms). (d) The isosurface of the potential energy, adapted from Mace et al. (2019) . . . . .	30
A.1	Flow Chart of the MATLAB program used. . . . .	36

# **CHAPTER 1. GAS TRANSPORT IN POROUS MEDIA AND LANGEVIN DYNAMICS**

Transport of gases and liquids in porous solid is important in various applications, both industrial and scientific, such as material synthesis, energy storage and water purification (Li et al., 2018). Different transport mechanisms, are known mechanical, electrical, magnetic and diffusive transport the latter will be of interest to us. Diffusive transport can be generated by differences in concentrations, pressures and/or by the effects of porous materials.

Porous materials are widely studied scientifically and in industrial applications, ranging from molecular separation to energy storage. They have open pore structures and a large surface area (including internal and external surfaces). The International Union of Pure and Applied Chemistry (IUPAC) classifies porous materials into three categories based on their pore diameter: those with pore diameters less than 2 nm are microporous; pore sizes between 2 and 50 nm are mesoporous; and pore diameters greater than 50 nm are called macroporous materials. "Nano" is a concept with a size of 1 to 100 nm; therefore, the above three types of porous materials are often also referred to as nanoporous.

Porous materials are of great interest due to their ability to interact with atoms, ions, molecules and nanoparticles not only at their external surfaces, but also inside the material. The presence of pores in nanostructured materials can enhance their physical and chemical properties. The understanding, design, and manipulation of pores has gained increased significance in current research.(Wang et al., 2013)

Improving the efficiency of porous media-based separations is critical to the advancement of many clean energy technologies, including gas and chemical separations, carbon capture and sequestration (CCS), water desalination, dehumidification, technology of fuel cells and electrochemical energy storage (EES). Schemes for designing highly selective species transport through microporous media have progressed considerably in the last decade due to the advent of microporous membrane components with controlled pore architectures and pore chemistry. The main classes of microporous materials are listed in Table 1.1.

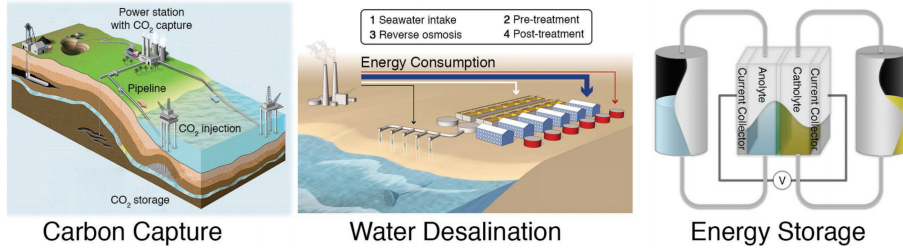


Figure 1.1: Example of microporous materials in new technological uses. Carbon capture. Water desalination and energy storage. Microporous membrane components include zeolites, MOFs, carbon nanotubes, organic nanotubes, and inherently microporous polymers. Adapted from Li et al. (2018).

Group	Example	Structure	Uses
Inorganic	Zeolites	Three-dimensional framework of tetrahedra	Ion exchangers in water purification
Hybrids	MOF	Organometallic Structures	energy storage
Carbons	carbon Nanotubes	Cylindrical	Gas and chemical separations

Table 1.1: Classes of microporous materials and their properties adapted from Cundy & Cox (2005), Stock & Biswas (2012), Saufi & Ismail (2004)

## 1.1 NANOTUBES

While much attention has been paid to the adsorptive and catalytic (Li et al., 2018) properties of large surface area microporous materials, In this Thesis we will discuss how the geometry of nanotubes impacts the diffusion-transport of N2.

Nanotubes are cylindrical structures, with diameters on the order of up to a few nanometers. Most nanotubes have a diameter of about one nanometer and can be many times longer ( $\approx 0.6\text{cm}$  (Zhu et al., 2019)). The structure of a nanotube can be conceptualized as the rolling of a hexagonal layer one atom thick into a cylinder (Figure 1.2).

Depending on the orientation of how the cylinder is wrapped, a nanotube can have different order in the positions of its atoms. There are three types of nanotubes according to the winding orientation: Armchair, ZigZag and chiral, where are illustrated in Fig. 1.3.

The most commonly studied nanotubes in material science are

- Gallium phosphide nanotubes (Mirzaei & Mirzaei, 2011b).
- Aluminum phosphide nanotubes (Mirzaei & Mirzaei, 2011a).
- Aluminum nitride nanotube (Noei et al., 2017), (Ganji et al., 2016) (Rouhi, 2016)
- Gallium nitride nanotubes (Rouhi, 2016)
- Boron nitride nanotube (Ganji et al., 2016)
- Carbon nanotube (Rouhi, 2016), (Dai, 2002), (Aqel et al., 2012)

Currently, the investigation of these nanotubes is focused on the search for interesting properties that are of interest for possible applications and on their synthesis. In general, these nanotubes can be used as a suitable material for optoelectronic applications due to their semiconductor-like behaviors.

In this thesis we focus on single-walled carbon nanotubes (SWCNT). Carbon nanotubes exhibit unique electrical, thermal and mechanical properties, and have also been used as molecular sieving materials (Dai, 2002). Catalysts, precursors, and process conditions can be adjusted to control nanotube diameters, either as single-walled or multi-walled nanostructures. (Li et al., 2018)

Nanotubes have a simple chemical composition and atomic bond configuration, but exhibit perhaps the most extreme diversity and richness among nanomaterials in terms of structure-property relationships, such as a pseudo regularity along the nanotube axis. SWCNTs exhibit some unique properties that have led to applications in various fields, including gas separations, gas storage, nanothermometers, DNA recognition, nanofluidic devices, and others. (Sokhan et al., 2004), (Cheng et al., 2001), (Williams et al., 2002). Because the inner diameter of the SWCN

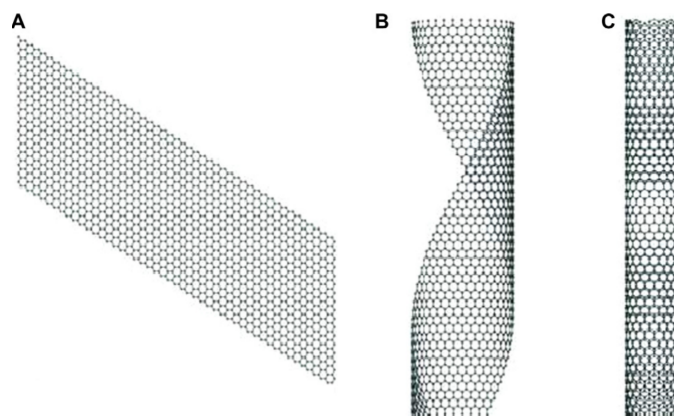


Figure 1.2: Rolling of a single layer sheet into a nanotube. Taken from Aqel et al. (2012)

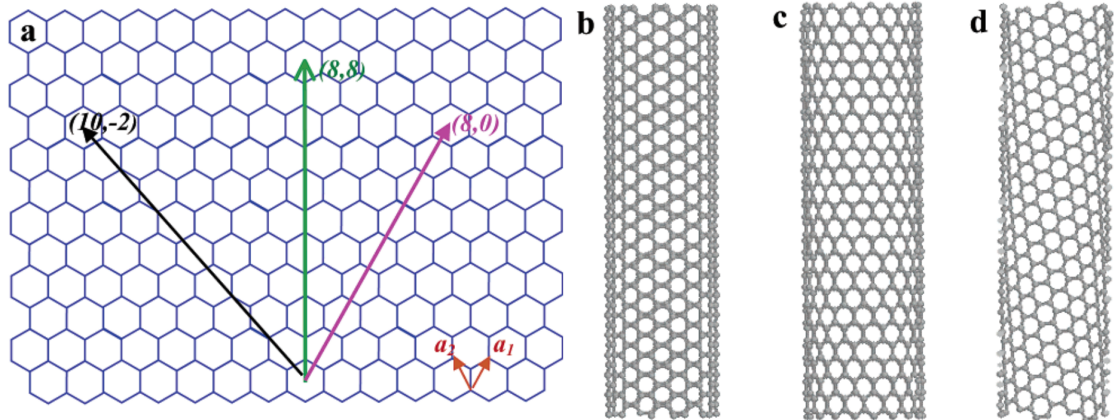


Figure 1.3: (a) Schematic structure of a sheet. Nanotubes can be formed by folding the sheet along lattice vectors. The two basis vectors  $a_1$  and  $a_2$  are shown. Folding of the  $(8,8)$ ,  $(8,0)$ , and  $(10,-2)$  vectors lead to armchair (b), zigzag (c), and chiral (d) tubes, respectively. Adapted from Dai (2002)

can be comparable to the size of the adsorbate, it is expected that the degree of adsorption and diffusion of the adsorbate in SWCNs are important functions of both the diameter of the nanotube and the adsorbate-nanotube interactions.

Depending on its chirality, SWCNTs can have as metals or semiconductors, with relatively small band gaps ( $\sim 0.5$  eV) for a typical diameter of  $1.5\text{nm}$  or large ( $\sim 10$  meV), even if they have almost identical diameters (Dai, 2002). For semiconductor nanotubes of the same chirality, the bandgap is inversely proportional to the diameter. Therefore, there are endless possibilities in the type of carbon tube “molecules”, and each nanotube could exhibit different physical properties. Since the discovery of the nanotube in 1952 (Monthioux & Kuznetsov, 2006), a theoretical and experimental effort has been made to discover the sensitivity of the electronic and mechanical properties of nanotubes on their atomic structures. The study and characterization of nanotubes have been greatly facilitated by the progress of their synthesis. While the extreme sensitivity of nanotube structure-property relationships has led to rich science and promises a wide range of applications, it is still a challenge for chemical synthesis in controlling the diameter and chirality of nanotubes.(Dai, 2002)

## 1.2 MOLECULAR SIEVING IN NANOTUBES

Molecular transport of fluids through porous media at the nanoscale is important in many industrial processes, including membrane filtration and separation (Figure 1.4).

Since the first calculations on the structure of fullerenes a few decades ago by

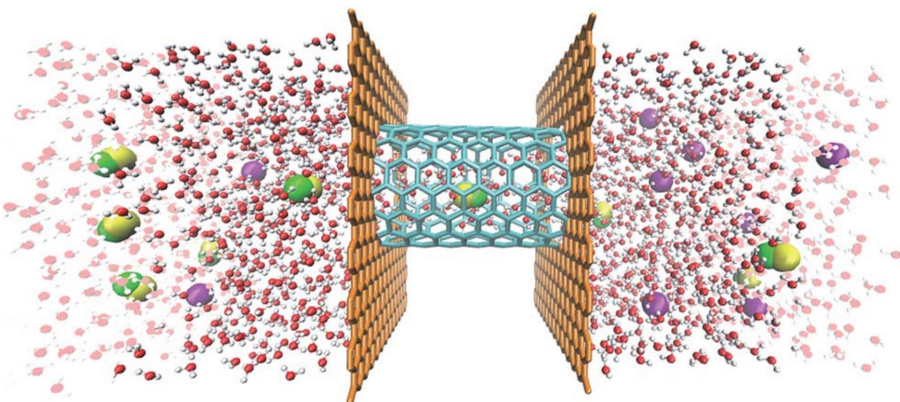


Figure 1.4: Simplified diagram of molecular separation. Taken from Khataee et al. (2017)

Pederson and Broughton Pederson & Broughton (1992) in which it was shown that nanotubes could attract fluids, there has been a continuing interest in developing methods to study adsorption on nanotubes. Following multiple reports on endohedral adsorption of hydrogen, it is reported that single walled nanotubes can adsorb hydrogen in significant amounts. Much work has been done to obtain experimental data for hydrogen storage capacities in single-walled carbon nanotubes. Despite the large variation in the reported data, it is clear that hydrogen is adsorbed on SWCNTs. Experimental evidence for adsorption of rare gases in nanotubes (Babaa et al., 2003) has also been reported. Researchers have synthesized endohedral structures containing various deposited metals from solution Tsang et al. (1994), and have predicted quantum sieving of hydrogen and neon into small diameter nanotubes (Wang et al., 1999).

Our current understanding of complex fluid transport processes in confined geometries relies heavily on computer simulations and experimental measurements in activated carbon, zeolites, silica gels, and activated alumina (Li et al., 2018). All of these porous materials are characterized by dispersion in pore sizes, including, for example, zeolites in which the effective pore diameter changes along the axis of the pores. In contrast, nanotubes offer a porous medium with a relatively defect-free surface and a well-defined internal diameter. Nanotubes are ideal candidates for molecular transport simulation studies in confined geometries, allowing their characteristics to be simplified to one dimension.

The mass transport of diatomic molecules, ie oxygen and nitrogen, has been investigated in graphitic slits with the conclusion that the diffusion rate is highly dependent on the slit width Travis & Gubbins (1999). Dependence of pore size on carbon transport properties Mixtures of dioxide and methane have also been reported for cylindrical graphitic pores (Nicholson, 2002). In general, mass transport in nanoporous structures depends on both the adsorbate-nanotube interactions and the thermodynamic state of the adsorbate in the confined medium, which is strongly affected by these interactions.

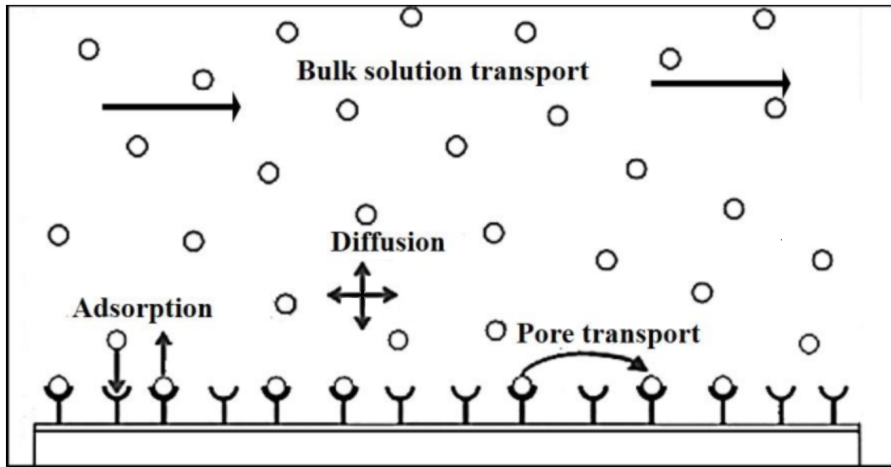


Figure 1.5: Simplified diagram of molecular transport. Effects of adsorption, transport in the pore, diffusion and bulk solution transport. Adapted from Moon (2019)

Taking Fig. 1.5 as an example, any pressure, temperature or concentration gradient leads a transport and/or movement of the gaseous solution towards a privileged direction. In our particular case, if the gas consists of a single type of molecule with constant temperature, pressure and concentration, the main factor to consider for transport under these conditions is the thermal interaction between the gas molecules with the nanotube molecules, thus generating a random motion (Brownian) of the gas molecules within the nanotube.

### 1.3 LANGEVIN TRANSPORT DYNAMICS

The seemingly random motion made by a particle immersed in a fluid is called Brownian motion. Brownian motion can be used as a basic model for the dynamics of non-equilibrium systems. The Langevin equation dominates the mechanism of brownian motion by considering friction forces and random forces. The fluctuation-dissipation theorem relates these forces to each other. This theorem has many important and powerful generalizations in statical physics.

For instance, the Langevin equation has been applied successfully to describe the movement of ions in water or the reorientation of dipole molecules (Zwanzig, 2001), and the instantaneous concentration of molecular components in a system that chemically reacts near thermal equilibrium. Lets us consider the one-dimensional motion of a spherical particle of radius  $a$ , mass  $m$ , position  $x$ , velocity  $v$  in a fluid medium with finite viscosity. Newton's equation of motion for the particle reads

$$m \frac{dv}{dt} = F_{tot}(t) \quad (1.1)$$

where  $F_{tot}(t)$  is the total instantaneous force on the particle. This force is due to the interaction of the Brownian particle with the surrounding medium. If the positions of the molecules in the surrounding medium were known as functions of time, then in principle this force is a known function of time.

However, an exact expression for  $F_{tot}(t)$  is generally not available. Interactions with the environment result in this force is a friction force proportional to the velocity of the Brownian particle, giving an equation of motion of the form

$$m \frac{dv}{dt} = -\gamma v \quad \rightarrow \quad v(t) = e^{-\frac{\gamma}{m} t} v(0) \quad (1.2)$$

where  $\gamma$  is called the viscous damping coefficient. From the solution we expect that the particle comes to rest at long times. However, we know that the root mean square velocity of a Brownian particle in thermal equilibrium is  $\langle v^2 \rangle_{eq} = KT/m$ , so the stationary velocity cannot be zero. Therefore, the assumption that  $F_{tot}(t)$  is given by a friction force only must be modified. The appropriate modification, suggested by the observed randomness of an individual particle trajectory, is to include the effect of a random or fluctuating force  $\delta F(t)$  to system. The equation of motion now reads

$$m \frac{dv}{dt} = -\gamma v + \delta F(t), \quad (1.3)$$

is Langevin's equation for a Brownian particle (Zwanzig, 2001). The total force is divided into a deterministic part (friction) and a random fluctuating part (noise). Both friction and noise result from the interaction of the Brownian particle with its environment (heat bath). There is a fundamental relationship between friction and noise.

There are two basic views on the nature of fluctuating force. In the most commonly discussed approach, the fluctuating force is assumed to emerge from occasional impacts of the Brownian particle with molecules of the surrounding medium. The force during an impact is assumed to occur over time scales much shorter than the relevant observation time.

The fluctuating force can be characterized by its first and second moments, relative to the time averages over an infinitesimal time interval. In general, first and second moments satisfy

$$\langle \delta F(t) \rangle = 0, \quad \langle \delta F(t) \delta F(t') \rangle = 2B\delta(t-t') \quad (1.4)$$

where the factor  $B$  can be considered as the intensity of the fluctuations. The delta function in time indicates that there is no correlation between impacts at different times. The mathematical

specification of this noise model is that of a fluctuating force with a Gaussian distribution. The results of a calculation using the Langevin equation are expected to be independent of the initial state and to include only the statistical distribution of noise. In this view, the averages in eq. 1.4 come from averages over initial states. As noted above, the particle velocity drops to zero in the absence of noise. In thermal equilibrium, we must demand that  $\langle v^2 \rangle_{eq} = kT/m$ . The stochastic Langevin equation can be solved, given the condition that the value of  $B$  must be equal to  $\gamma k_b T$ .

This result is known as the fluctuation-dissipation theorem. It relates the intensity  $B$  of the random noise or fluctuating force to the magnitude of the friction or dissipation  $\gamma$ . It expresses the balance between friction, which tends to bring any system to a completely “dead” state, and noise, which tends to keep the system “alive”. This equilibrium is required to have a state of thermal equilibrium over long periods of time (Zwanzig, 2001).

## 1.4 DIFFUSION COEFFICIENT FROM STOCHASTIC DYNAMICS

Diffusion is a fundamental mechanism of molecular transport through porous media. Diffusive transport occurs for example when two parts of the pore are connected by reservoirs at different pressures (different chemical potentials) and describes, therefore, an irreversible process, analogous to friction. In confined systems, diffusion is general anisotropic and the corresponding phenomenological transport diffusivity is a tensor, the trace of which is generally different from the corresponding bulk scalar value (Sokhan et al., 2004). Diffusion of a particle in a solid state crystalline host material is determined by a complex interaction between particle-host, particle-particle, and host-host interactions. From a scientific point of view, the diffusion of a mobile species within a crystalline material can be considered a hopping motion from one site to another, in a rigid network of sites.

A consequence of the fluctuation dissipation theorem is the connection between the velocity correlation function and the diffusion coefficient (Zwanzig, 2001). Working with the velocity of a particle can sometimes be easier than working with the mean square displacement, as in our case. The velocity correlation function is an equilibrium average and cannot depend on any arbitrary origin of the time axis. It can depend only on the time difference  $t - s = u$ , so that

$$\frac{\partial}{\partial t} \langle x^2 \rangle = 2 \int_0^t ds \langle v(t-s)v(0) \rangle = 2 \int_0^t du \langle v(u)v(0) \rangle \quad (1.5)$$

The velocity correlation function generally decays to zero in a short time. The diffusion equation is valid only in time periods much longer than the characteristic molecular time. In the limit of large  $t$ , the left-hand side approaches  $2D$ , and the right-hand side approaches a time integral

from zero to infinity, so we have derived the simplest example of the relation of a transport coefficient to a time correlation function

$$D = \int_0^\infty dt \langle v(t)v(0) \rangle \quad (1.6)$$

For the special case for the simple Brownian motion, the autocorrelation function is:

$$\langle v(t)v(0) \rangle = \frac{k_b T}{m} e^{-\gamma t} \quad (1.7)$$

where, in this case the decorrelation time coincides with  $\tau = 1/\gamma$ . The diffusion coefficient is inverse proportional to  $\gamma$  and given by (Goga et al., 2012)

$$D = \frac{k_b T}{m\gamma} \quad (1.8)$$

So far we have only dealt with the diffusion of a free particle. If we extend the equation 1.6 to a system of particles, we can calculate the diffusion of the system as:

$$D = \frac{1}{N_p} \lim_{t \rightarrow \infty} \sum_{i=1}^{N_p} \int_0^t d\tau \langle v_i(0)v_i(\tau) \rangle \quad (1.9)$$

Where  $N_p$  is the total number of particles in the system. From the trajectories of  $N_p$  particles in a ensemble, the mean square displacements (MSD) can be defined as

$$MSD = \langle (r(t) - r(t_0))^2 \rangle = \frac{1}{N} \sum_{i=1}^N (r_i(t) - r_i(t_0))^2 \quad (1.10)$$

As long as the simulations are performed on a time scale long enough to achieve the diffusion rate, the self-diffusion coefficients  $D_s$  can be calculated according to equation

$$D_s = \frac{1}{2a} \lim_{t \rightarrow \infty} \frac{d}{dt} \langle (r(t) - r(t_0))^2 \rangle \quad (1.11)$$

for  $a$  dimensions. The diffusion coefficient  $D_s$ , can be calculated from the slope of the mean-squared displacement versus time plot. Care must be taken to simulate long enough and to consider only the linear diffusive regime, where the mean-squared displacements are not correlated with short-timescale ballistic motion (Arora et al., 2004) (Bukowski et al., 2021). This mentioned link between Brownian motion and diffusion, and the technological advance of computers, has made it possible to study diffusion processes at all scales. Alder and Wainwright were the first to perform a molecular dynamics simulation where the trajectories of individual particles are tracked over time by integrating the Newtonian equations of motion from the interatomic forces of individual molecules over time. (Bukowski et al., 2021). In porous media, there also exists a sub-diffusive

region that is correlated with pore wall collisions.

By calculating  $D_s$  at different temperatures  $T$ , we can extrapolate the diffusion activation energy  $E_a$  and the temperature-independent preexponential  $D_0$  with an Arrhenius diagram according to equation:

$$D_s = D_0 e^{\frac{-E_a}{k_B T}} \rightarrow \ln(D_s) = \ln(D_0) - E_a/k_B T \quad (1.12)$$

Therefore, the calculation of activation energy requires several simulations separated by structure on the nanosecond time scale for diffusion involving activated processes (Mace et al., 2019).

## CHAPTER 2. COMPUTATIONAL LANGEVIN DYNAMICS

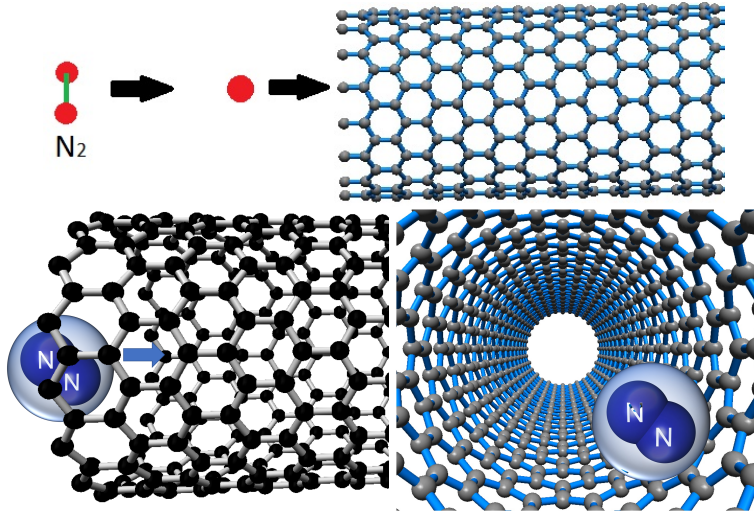


Figure 2.1: Simplified diagrams of the problem

Molecular Dynamics of three-dimensional transport of gases in single wall carbon nanotube (SWCNT) are computationally expensive. In this Thesis we take advantage of the regular characteristics of the SWCNT to search to look for an alternatives way of reducing the complexity of the simulations using Langevin's algorithm, considering a reduction in dimensionality (3D to 1D) taking into account only the axial potential of the nanotube. The diatomic nature of nitrogen is neglected and is taken as a solid sphere, with the mass of  $N_2$  neglecting the rotation, oscillation and angles between the nitrogen molecules and an effective Leonard Jonnes-type potential will be used taking into account the above conditions. The interactions between nanotubes and nitrogen will be governed by randoms kicks quantified by the parameter  $\gamma$ . Our goal is to show that for a convenient choice of the damping parameter  $\gamma$ , we can reproduce previous results in the literature of the self-diffusion coefficient.

Arora et al. (2004) performed Gran Canonical Monte Carlo (GCMC) simulations of the adsorption and diffusion of  $N_2$  molecules within a SWCNT of different diameters (SWCNT from (11,0) to (20,0)), and at 100K and 298K. Figure 2.2a shows the effective radial potential of (15,0) SWCNT calculated and used in those simulations where we can see that it has 2 minima of equal depth at a radius of  $\approx 2.5\text{\AA}$ . The Figure 2.2b Mean square displacements for nitrogen in SWCNs on a log-log plot to verify that it is in the non-ballistic diffusion regime. Figure 2.2c show pressure where it is estimated at which point saturation of the system is achieved. Figure 2.2d show nitrogen self-diffusion in (15,0)SWCN as a function of load where they used EMD simulations to calculate them. The interactions between particles were calculated according to the Lennard-Jones potential and the molecular bonds are also considered a harmonic potential  $N_2$  for the vibrational motion.

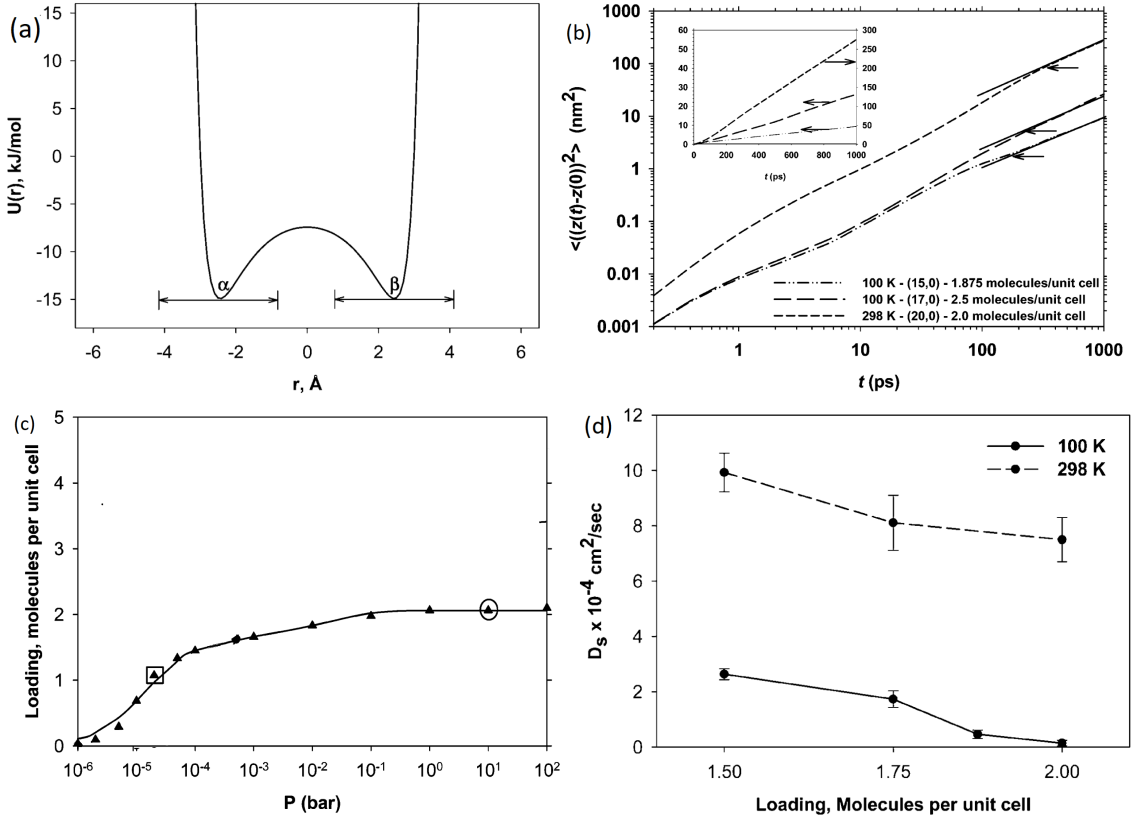


Figure 2.2: (a) Radial potential SWCNT (15,0), (b) Mean square displacements for nitrogen in SWCNs on a log-log plot, (c) Loading vs pressure SWCNT (15,0), (d) Nitrogen self-Diffusion in SWCN as a function of load. Figure taken from Arora et al. (2004)

Sokhan et al. (2004) studied the transport properties, diffusivities of a diatomic molecule within a SWCNT by means of molecular dynamics in equilibrium at different temperatures and as a function of pressure. Sokhan et al. (2004) studied the autocorrelation function of the speed of translation and rotation of diatomic molecules. The vertical dashed line on the 100 K bulk isotherm denotes a gas–liquid phase transition. They found a vertical dashed line on the 100 K bulk isotherm, that denotes a gas–liquid phase transition.

## 2.1 STOCHASTIC MOLECULAR DYNAMICS ALGORITHM

There are several alternative computational methods to study the dynamics of classical interacting particles under different conditions. Techniques for simulating diffusion using atomistic models can be generally classified into two groups: those that follow molecular trajectories over time and those that sample the free energy surface and use transition state theory (TST) to calculate the diffusion rate. Generating molecular trajectories is the more intuitive

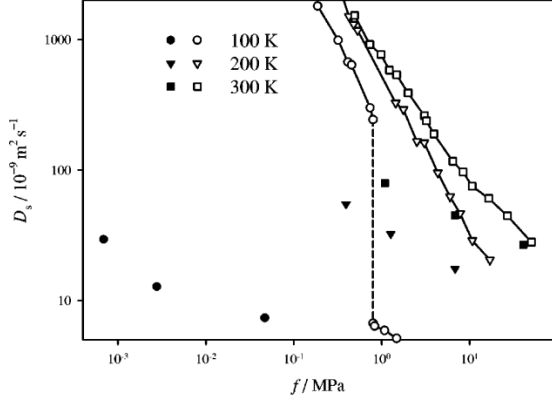


Figure 2.3: Diffusion and pressure, where a phase transition is observed at 100K. Taken from Sokhan et al. (2004)

approaching. The molecular dynamics (MD) simulation technique the forces the act on each atom in the system are evaluated at each step of time. The particle's positions and velocities are updated are based on Newton's equations of motion. In the quest to perform more realistic simulations, more accurate expressions for potential energy are needed to calculate forces. In classical MD simulations, the potential energy is typically described as a sum of terms describing bond stretching, bond angle bending, torsional potentials, and non-bonded interactions, such as dispersion, repulsion, and Coulombic forces.

The accuracy of a simulation is typically more sensitive to the accuracy of the Lennard–Jones parameters and partial charges than to the bonded interactions, such as bond stretching. The Newtonian equations can be integrated numerically using a variety of different integration schemes. Typical time steps are  $\approx 1fs$ , and with modern computers MD can simulate times scales of tens of nanoseconds routinely. In order to estimate the diffusion of a molecule of  $N_2$  quickly and easily, we modify the MD algorithm, by adding a stochastic component (explained in Sec. 1.3). This stochastic component attempts to artificially reproduce the effects of thermal interactions, collisions between nitrogen molecules and nanotube, bond oscillations and  $N_2$  rotations.

In Appendix A we schematically explain the general steps of the program made in MATLAB represented in the flow diagram Fig.A.1.

### 2.1.1 Verlet leap frog algorithm

Despite its low order, the method has excellent energy conservation properties and is widely used. If  $h = \Delta t$  denotes the size of the timestep used for the numerical integration, then

the integration formulae applied to each component of an atom's coordinates and velocities are

$$v_{i_x}(t + \frac{1}{2}h) = v_{i_x}(t - \frac{1}{2}h) + ha_{i_x}(t) \quad (2.1)$$

$$r_{i_x}(t + h) = r_{i_x}(t) + hv_{i_x}(t + \frac{1}{2}h) \quad (2.2)$$

The name 'leapfrog' stems from the fact that coordinates and velocities are evaluated at different times; if a velocity estimate is required to correspond to the time at which coordinates are evaluated, then

$$v_{i_x}(t) = v_{i_x}(t - \frac{1}{2}h) + \frac{1}{2}ha_{i_x}(t) \quad (2.3)$$

can be used. The local errors introduced at each timestep due to the truncation of what should really be infinite series in  $h$  are of order  $O(h^4)$  for the coordinates and  $O(h^2)$  for velocities. The leapfrog method can be reformulated in an alternative, algebraically equivalent manner that enables the coordinates and velocities to be evaluated at the same instant in time, avoiding the need for the velocity adjustment in 2.1.1. To do this, the computations are split into two parts: Before computing the acceleration values, update the velocities by a half timestep using the old acceleration values, and then update the coordinates by a full timestep using the intermediate velocity values,

$$v_{i_x}(t + \frac{1}{2}h) = v_{i_x}(t) + \frac{1}{2}ha_{i_x}(t) \quad (2.4)$$

$$r_{i_x}(t + h) = r_{i_x}(t) + hv_{i_x}(t + \frac{1}{2}h) \quad (2.5)$$

Use the new coordinates to compute the latest acceleration values and update the velocities over the second half timestep,

$$v_{i_x}(t + h) = v_{i_x}(t + \frac{1}{2}h) + \frac{1}{2}ha_{i_x}(t + h) \quad (2.6)$$

### 2.1.2 Impulsive Langevin Leap-Frog algorithm

We solve for the position  $x(t)$  and velocity  $v(t)$  considering a stochastic component in the velocity using a variant of the Verlet algorithm called "Impulsive Langevin Leap-Frog algorithm" (Goga et al., 2012). The algorithm considers a system of  $N$  particles with  $3N$  degrees of freedom, and considers every degree of freedom separately. We assume  $v(t - (1/2)h)$ ,  $x(0)$  and  $F(t) = ma$  are the known velocity, coordinate and force components, and  $a$  is the acceleration at time  $t$ . For all

the degrees of freedom, execute these steps:

1.  $v = v(t - \frac{1}{2}h) + ah$
2.  $\Delta v = -fv + \sqrt{f(2-f)(k_b T_{ref}/m)\xi}$
3.  $x(t + \frac{1}{2}h) = x(t) + v\frac{1}{2}h$
4.  $x(t + h) = x(t + \frac{1}{2}h) + (v + \Delta v)\frac{1}{2}h$
5.  $v(t + \frac{1}{2}h) = v(t) + \Delta v$

where  $h = \Delta t$  and  $a$  is:

$$a(t) = \frac{F(r(t))}{m} \quad (2.7)$$

Step 1 is the ordinary MD velocity-update, the step 2 is the impulsive application of friction (reducing the velocity  $f = 1 - e^{-\gamma h}$ ) and noise ( $\xi$  is a random number taken from a normal distribution). The Step 3 and 4 updates the coordinates. Step 4 assigns the modified velocity to the velocity at the end of the time step.

It is interesting to work with this algorithm because it implements a parameter  $\gamma$  for dissipation and random kicks, which is capable of storing all the information of intermolecular and thermal collisions between a nitrogen molecule and a nanotube. This way, by finding the parameter  $\gamma$  that fits the experimental diffusion curves, it is possible to determine what would be the collision rate per unit of effective second that the experimental diffusion represents.

When considering many particles, we have to implement the interaction potentials between these LJ-type molecules so that they collide with each other. The application of the interparticle interaction in pairs ensures the conservation of linear momentum, both globally and locally at distances on the order of the interaction range of the particles. Some aspects to take into account in these collisions are the geometry and impact angles, where according to these conditions the momentum of the particles involved can be transmitted in different ways. In this thesis, this behavior will only be treated in its simplest one-dimensional form, to work on a plane or in 3D space, see Goga et al. (2012). A short-range list of pairs of molecules is used. The distance dependence can be chosen arbitrarily; the originally suggested method chooses a linear dependence between  $r < r_c$  (collision probability) and  $r > r_c$  (zero collision probability). After determining the change in relative velocity due to impulsive friction and noise, this change is distributed between the two particles such that the center of mass is conserved. The selection of pairs can be done in several ways. In principle, all neighbors can be selected (this would correspond to the original procedure), but it is sufficient and much more efficient to select only one (or a few) neighbors per particle. The selection can be done randomly, but can also be based on a distance-weighted probability, for example, proportional to  $1 - (r_{ij}/r_c)$  which is used in this thesis.

A selected torque can be subjected to friction and corresponding noise, with friction isotropically distributed in the direction of speed. It is also possible to combine more than one choice. Different options can be applied to the same pair of particles, but each option can also be applied to a different pair, depending on their privileged geometries and directions after collisions.

For each pair  $i, j$  selected with velocities  $v_i$  and  $v_j$ , the following is done:

1. Calculate the speed reduction factor  $f$ , as described above.
2. Determine the velocity noise factor  $g$ , defined as

$$g = \sqrt{f(2-f)k_B T / \mu} \quad (2.8)$$

where

$$\mu = \frac{m_i m_j}{m_i + m_j} \quad (2.9)$$

is the reduced mass of the pair.

3. Construct the relative velocity vector  $v$  of the selected pair:

$$v = v_i - v_j \quad (2.10)$$

4. Choose a random numbers  $\xi$  from a standard normal distribution (mean = 1, sd = 1) and construct the vector:

$$\Delta v = -fv + g\xi \quad (2.11)$$

5. Distribute the relative velocity change over the two particles:

$$v_i = v_i + \frac{\mu}{m_i} \Delta v \quad (2.12)$$

$$v_j = v_j - \frac{\mu}{m_j} \Delta v \quad (2.13)$$

In this way, the velocities of the particles are updated while the total momentum  $m_i v_i + m_j v_j$  is conserved. Note that the particle velocities are updated after each impulsive event, not at the end of each step. This is necessary, as a single particle may be involved in more than one pair event. First adding the velocity changes and then updating the velocities with the sum of the velocity changes gives erroneous results.

### 2.1.3 Flying Ice cube effect

The "Flying Ice Cube Effect" was initially used as a term that describes the violation of the equipartition theorem caused by speed scaling procedures. Some of the possible manifestations of this effect are the accumulation of kinetic energy in translational or vibrational degrees of freedom or the development of temperature gradients. The flying ice cube effect is an artificial situation found in molecular dynamics simulations (Braun et al., 2018).

In particular for our simulation, this artificial effect of movement is reflected in a collective movement of all the particles towards one direction moving as if the system was a sliding solid (this is where the name comes from). This effect creates a synthetic addition in speed, affecting the energy of the system and altering the calculation of self-diffusion (Ec.1.9). To eliminate this effect in our simulation, we just subtract the velocity of each particle " $v_i$ " from the velocity of the center of mass " $v_{mc}$ ".

$$v_{i_{New}} = v_i - v_{mc} \quad (2.14)$$

where the velocity of the center of mass is the average of the velocity of all the particles.

### 2.1.4 Lennard-Jones Potential

The Lennard-Jones potential consists of two parts, a repulsive term ( $r^{-12}$ ), and attractive term ( $-r^{-6}$ ), representing the London dispersion forces. Apart from being an important model in itself, the Lennard-Jones potential frequently forms one of 'building blocks' of many force fields. It is worth mentioning that the 12-6 Lennard-Jones model is not the most faithful representation of the potential energy surface, but rather its use is widespread due to its computational expediency. The Lennard-Jones potential is a function of the distance between the centers of two particles. The particles come closer together until they reach a region of separation where the two particles become bound, their bonding potential energy decreases from zero to a negative quantity. While the particles are bound, the distance between their centers continue to decrease until the particles reach an equilibrium, specified by the separation distance at which the minimum potential energy is reached. If the two bound particles are further brought together, past their equilibrium distance, repulsion begins to occur: the particles are so close to each other that their electrons orbitals repel. Given the repulsive force between both particles, their binding potential energy increases rapidly as the distance of separation decreases.

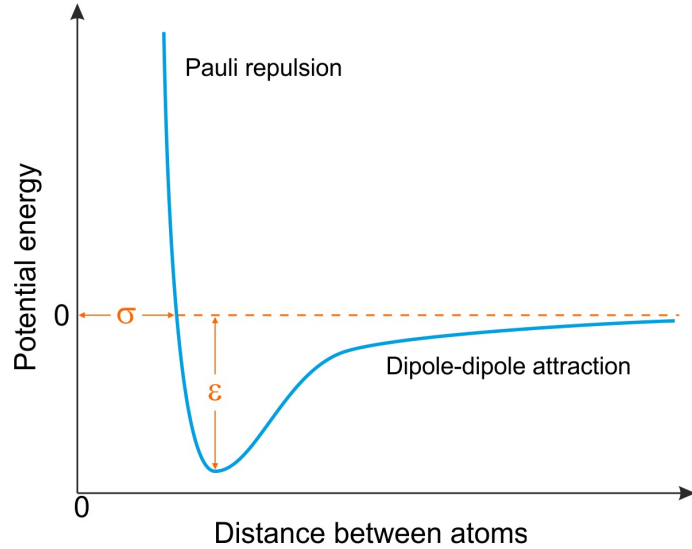


Figure 2.4: Plot of the Lennard-Jones potential function: Intermolecular potential energy as a function of the distance of a pair of particles.

$$V(r) = 4\epsilon \left[ \left( \frac{\sigma}{r_{ij}} \right)^{12} - \left( \frac{\sigma}{r_{ij}} \right)^6 \right] \quad (2.15)$$

where  $r_{ij}$  is the distance between two interacting particles,  $\epsilon$  is the depth of the potential well, and  $\sigma$  is the distance at which the particle-particle potential energy  $V$  is zero (often referred to as 'size of the particle'). The Lennard-Jones potential has its minimum at a distance of  $r = r_{min} = 2^{1/6}\sigma$ , where the potential energy has the value  $V = -\epsilon$

## CHAPTER 3. NITROGEN DIFFUSION IN CARBON NANOTUBES

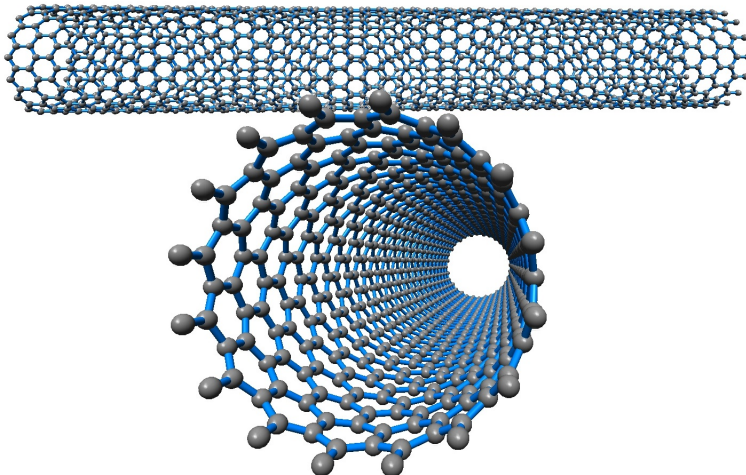


Figure 3.1: Three-dimensional model of the carbon nanotube used. (15,0)

The SWCNT analyzed in this Thesis were created from XYZ files exported from the Nanotube Modeler program (Nanotube-Modeler, 2004-2005). We used a Zig Zag (15,0) SWCNT with 1215 carbon atoms, 85.2 Å long and 6.268 Å radius and 1.421 Å between C-C (Fig.3.1), with a total time simulation 5 ns and 1 fs of time step. As we want to know the dynamics of the molecules in a one dimension (axial Potential) we must look for which path is the most likely to travel by a molecule of  $N_2$ , for this, we first calculate the potential along the radial radial axis as discussed in Sec.2.1.4. By determining the minimum of the potential, it will be possible to find at which point of the radial distance the molecules are most likely to move. The potential difference at each point of the axial axis will be taken into account.

As initial conditions, the  $N_2$  molecules will be pseudo-uniformly distributed along the axial axis of the nanotube, but with a small random displacement from each other. We set periodic boundary conditions at the ends of the nanotube, in such a way that the  $N_2$  molecules are able to interact with molecules at the other ends. With the conditions set, we let the system evolve with the stochastic Verlet algorithm discussed in Chapter 2.

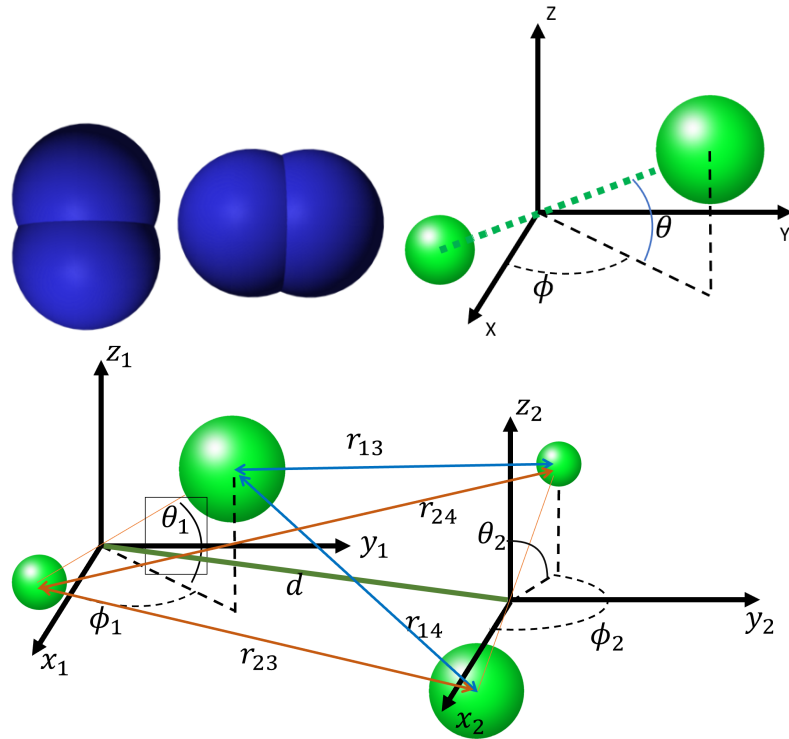


Figure 3.2: Representation of the orientations that nitrogen can adopt. For each configuration, different potentials are obtained as a function of their distances from their respective centers of mass.

	N-N	C-N
$\sigma[A]$	3.32	3.36
$\epsilon/k_B[K]$	36.4	33.4

Table 3.1:  $C - N$  and  $N - N$  Lennard-Jones interaction parameters taken from Arora & Sandler (2006),Bojan & Steele (1987).

### 3.1 NITROGEN-NANOTUBE INTERACTION POTENTIAL

The system we wish to analyze consists of a SWCNT which interacts with a  $N_2$  and  $N_2 - N_2$ , in the Section(2.1.4) it was mentioned about the Lennard Jones potential. In the literature (Arora et al., 2004) the C-N and N-N interaction parameters are given by Table.3.1.

To correctly model the dynamics of the particles, we need to find an effective total potential (both for  $N_2 - N_2$  and  $C - N_2$ ) which is capable of perceiving the different spatial orientations that the bimolecular nature of nitrogen can adopt (Fig.3.2).

By adding linearly the interactions between each pair of molecules ( $r_{13}, r_{14}, r_{23}, r_{24}$ ) for random orientations of each molecule and then averaging with a Boltzman weighing (Ec. 3.1), it is possible to find an effective total potential (Fig.3.2).

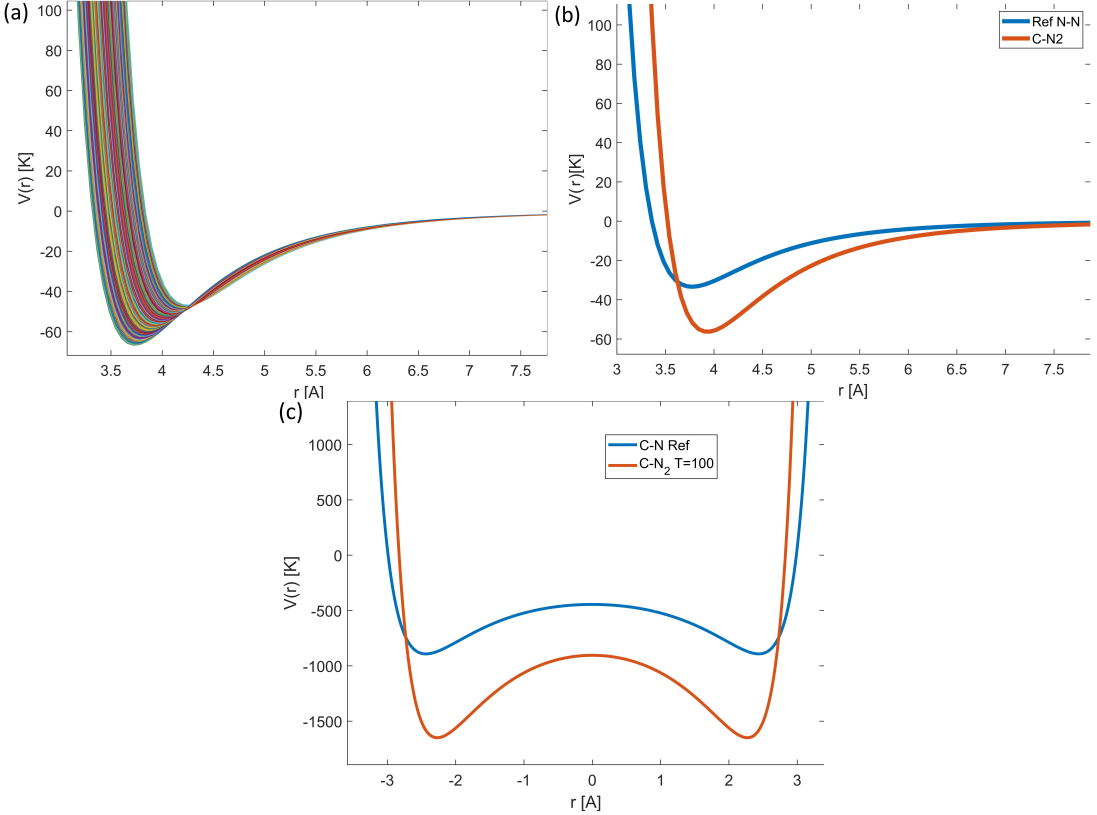


Figure 3.3: Potential  $C – N_2$  in Kelvin. (a) Potentials as a function of the distance between Carbon and the center of mass of  $N_2$ . Each curve (5000) is a potential with random orientations of  $N_2$ . (b) Blue. Potential as a function of the distance between Carbon and Nitrogen according to table 3.1. Red. Potential as a function of distance at 100K weighted with the equation (3.1) of 5000 possible orientations. (c) Blue. Potential as a function of the radius between Carbon and Nitrogen according to table 3.1. Red. Potential as a function of radius with the potential calculated in the previous Figure 3.3

$$V(T, d) = \frac{\sum_i e^{\frac{-\min(V_i(d))}{k_B T}} \cdot V_i(d)}{\sum_i e^{\frac{-\min(V_i(d))}{k_B T}}} \quad (3.1)$$

Then we must calculate (Eq. 3.1) a new effective potential (Fig.3.3b) that considers the possible spatial orientations of the diatomic molecule (Fig.3.3a) .

Knowing the interaction potential between  $C – N_2$ , we can calculate the potential as a function of the radius of the interior of the nanotube (Fig.3.3c). With the potential seen in Fig.3.3c, we can make the first comparison with the literature, with the radial potential described by Fig.2.2a, where we can see that the minima have been located at the same distance and qualitatively similar characteristics. We can see the behavior of the potential in a radial cut of the nanotube to verify the consistency and difference of the potential along the axes in the Figure 3.4. (Remember that the radius of the nanotube is 5.876 Å and that these graphs are cropped to appreciate the differences in potentials).

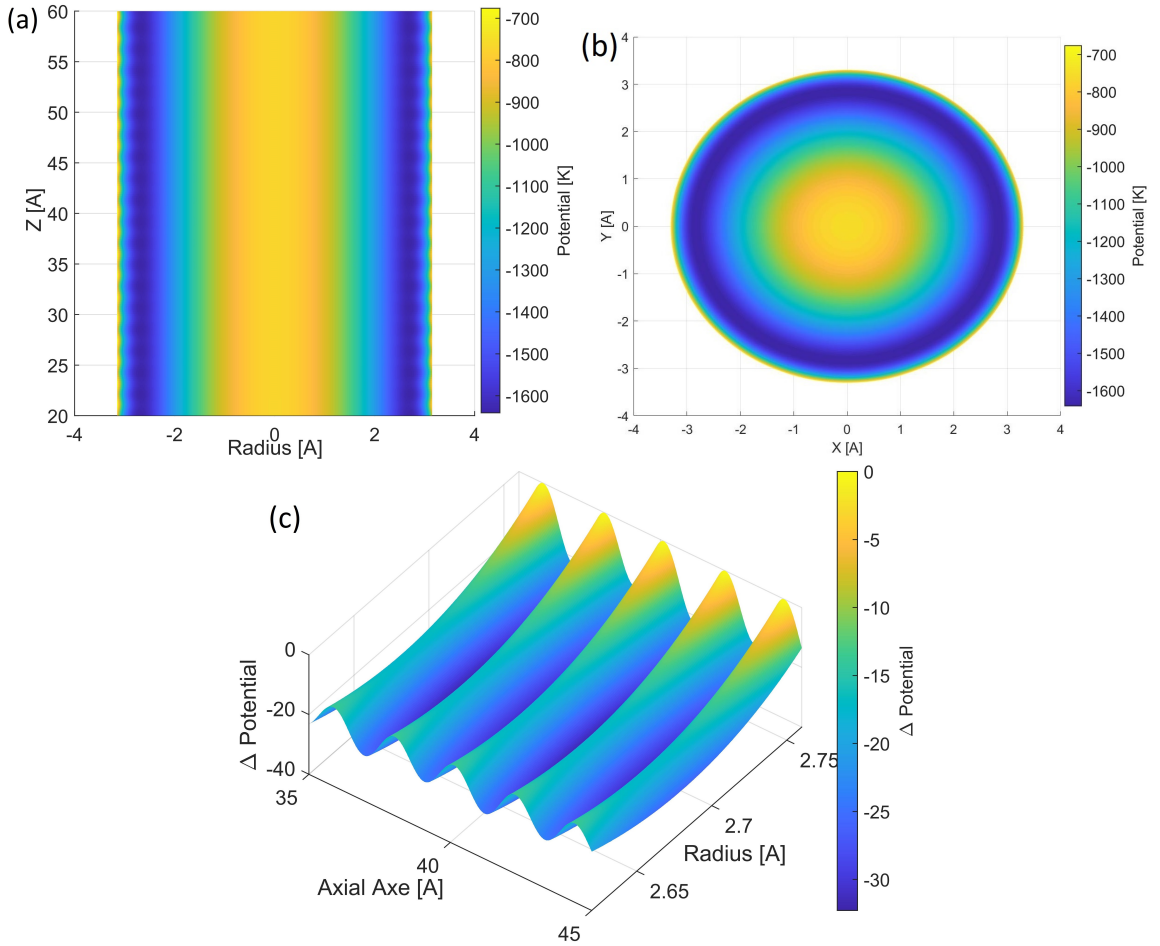


Figure 3.4:  $N_2 - C$  Potential energy in Kelvin of the Zig Zag nanotube (15,0) with radius of 5.87 Å. (a) Axial Potential within the nanotube. (b) Representation Radial-Azimuthal potential. (c) Magnification in a small region of the nanotube, around the minimum of the radial potential.

In the Fig.3.4 we see that the minima are in line at a fixed radius, there are minimal azimuth differences, and that along it, it has small oscillations. Taking this minimum radial potential as a reference to calculate the axial potential of a single isolated nanotube, we obtain Fig. 3.5a. But since our objective is to obtain the diffusion inside the nanotube without considering the effects of the edges of the tube (periodic edge conditions in the axial axis), we can only keep the uniform part of the potential located in the center of it, obtaining the Fig.3.5b.

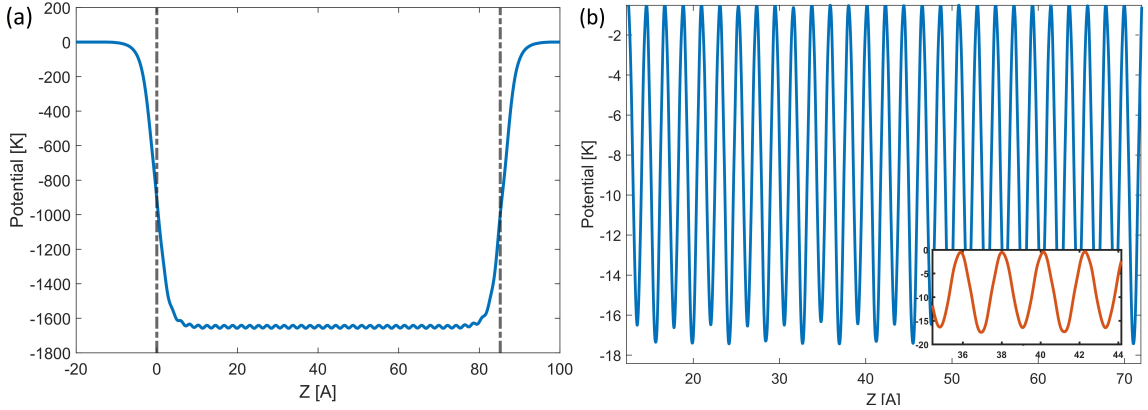


Figure 3.5:  $N_2 - C$  Axial Potential energy in Kelvin.(a) Blue: Axial potential of an isolated nanotube. Black: Limitation of where the nanotube would be found. (b) Blue: Axial potential along the minimum in the nanotube. Inset: Close up of the image of the potential with a periodicity of  $2.15\text{\AA}$  between minima.

The calculated axial potential is approximately 17K deep, and as additional data, a periodicity between minima of  $2.15\text{\AA}$ ] can be observed. With the potential found in the Fig.3.5b, we work on the following sections.

### 3.2 INTERMOLECULAR POTENTIAL

We have to find the effective potential between the diatomic molecules of  $N_2$ , if we simulate a large set of potentials of  $N_2 - N_2$  considering all possible configurations or orientations with equal probability we obtain Fig.3.6a. To better understand the effect of temperature on the potential, seven potentials were obtained at different temperatures with the average defined in Eq.1.9.

As can be seen in the Fig.3.6b, we see that at a lower temperature, the equilibrium distance between  $N_2 - N_2$  is smaller and that the minimum potential is considerably deeper. On the contrary, if we observe the curves with more temperature, we observe that the equilibrium distance is greater and that the minimum of the potential is more superficial.

This effect is easily explained if we consider the effect of the spatial orientations of the  $N_2$  molecules. At low temperatures, the possible spatial orientations that the  $N_2$  molecule experiences are "limited". They are arranged in such a way as to minimize energy. The opposite is the case at high temperatures that experience almost equally all possible spatial orientations, including (for example) a system of two interacting  $N_2$  molecules arranged collinearly in space (system where energy is maximized).

Finally, finding the minima of the potentials and their intersection with zero, we can

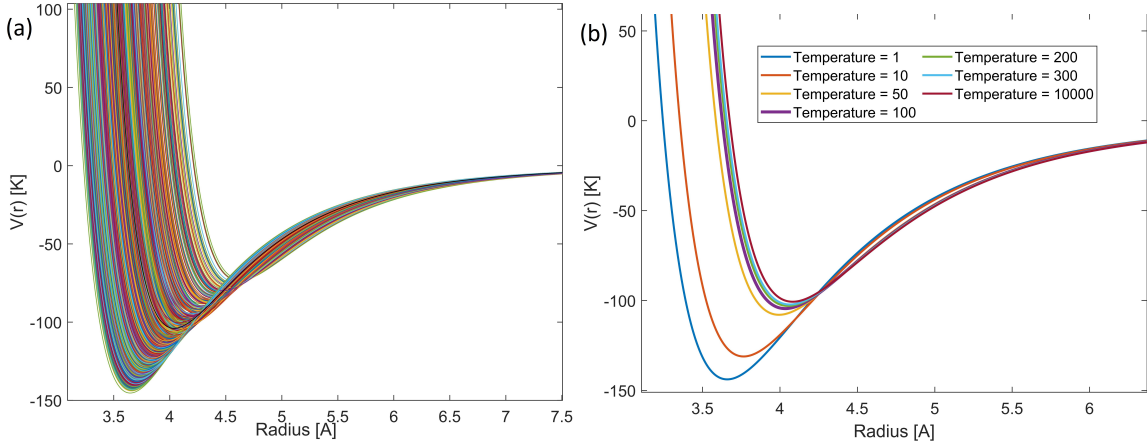


Figure 3.6:  $N_2 - N_2$  Potential energy in Kelvin. (a) Potentials as a function of the distance between  $N_2 - N_2$ , each curve (5000) is a potential with random orientations. (b) Potential as a function of the distance between  $N_2 - N_2$  at different temperatures

	$N_2 - N_2$	$C - N_2$
$\sigma$ [Å]	3.627	3.522
$\epsilon/k_B$ [K]	104.495	56.24

Table 3.2:  $C - N_2$  and  $N_2-N_2$  Lennard-Jones interaction parameters at T=100K

determine its Lennard Jones potential analogue, the parameters obtained are found in the Table3.2

As the  $\sigma$  parameter can be considered as the average "radius" of the studied molecule, from the Table3.2 we find that the nitrogen molecule is greater than the distance between the minimum radial potential, which can provide us with the information that on average it is unlikely that two molecules of  $N_2$  are in the same axial position which at the same time means that it is unlikely that these molecules are interchanged, favoring movement only along the axial axis.

### 3.3 SINGLE MOLECULE DIFFUSION

The next step out is to determine the  $\gamma$  parameter that we must use as input. One way to find a suitable value is to use a specialized program in molecular dynamics, such as LAMMPS (Atomic & Simulator, 2013) to compute the diffusion as a function of temperature. Since we know that the potential in the axial direction does not exceed 17.4K, we can approximate the diffusion at high temperature as that of a free particle given by the equation (1.8). The details of the simulation input carried out in LAMMPS can be found in the Appendix B.

As shown in the Fig.3.6 where it was the particular case of  $N_2 - N_2$ , it happens very similarly for the case of the C-N interaction, where at temperatures greater than 100K, the C-N

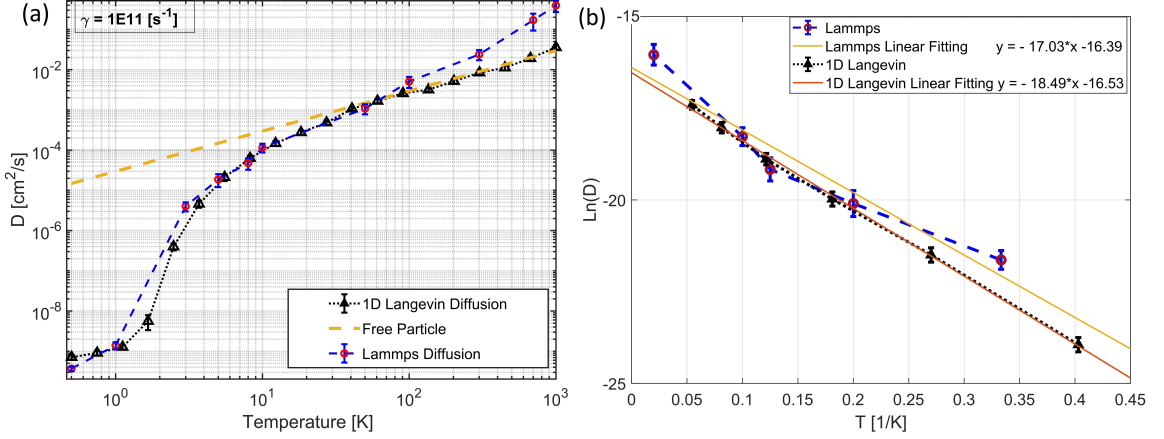


Figure 3.7: (a) Diffusion vs Temperature. Yellow: Theoretical free particle diffusion (1) as a function of temperature with  $\gamma = 0.1$  THz. Black: 3D simulated diffusion MD one-particle (1) as a function of temperature. Blue: 1D Langevin simulated diffusion one-particle as a function of temperature. (b)  $1/T$  Vs  $\ln(D)$  of the diffusion obtained with our program and those of the lams and their respective linear fitting, where the slope corresponds to the activation energy ( $K$ ) according to eq.1.12

potential quickly converges to the effective potential of a high temperature. So our results can be considered good approximations using the  $C - N_2$  potential obtained at  $T = 100K$  in the previous section.

The data obtained from diffusion vs temperature of LAMMPS (Fig.3.7a Blue) agree that the  $\gamma$  parameter that will be used in the Langevin algorithm should be approximately 0.1 THz. Using this parameter in our program, we obtain the black curve. From Fig.3.7a, we observe that both curves behave qualitatively in a similar way, achieving a similarity of the diffusions in a medium temperature range (10-100K). Outside the mid-temperature range, we see a discrepancy in the data due to different effects. At low temperatures ( $< 10K$ ), we observe that the diffusion predicted by the 1D langevin algorithm is greater than that calculated with DM, this is because the diffusion calculated with 1D langevin is using the potential of the SCWNT at 100K, but remembering the effect of temperature in the calculation of the potential, we find that the axial potential would actually be much deeper than the one used, implying less diffusion. At high temperatures ( $> 200K$ ), we observe that the diffusion calculated with 1D Langevin is smaller than that calculated with DM, in this case, the effect to be considered is the overcoming of the radial potential barrier found in the center of the nanotube (Fig.3.3c). At higher temperatures, the nitrogen molecules now can be located in the center of the nanotube, obtaining a greater cross-sectional area through which the nitrogen molecule can move; which is not allowed in a 1D Langevin model.

If we use the data of the diffusion obtained with our program and those of LAMMPS, we can obtain the activation energy of the axial potential comparing with the equation1.12, we obtain the Fig.3.7b, where it is determined that the activation energy at lower temperatures (where the potential of nanotubes is dominant 3-30K) has a value of  $17.03K$  for LAMMPS simulation and

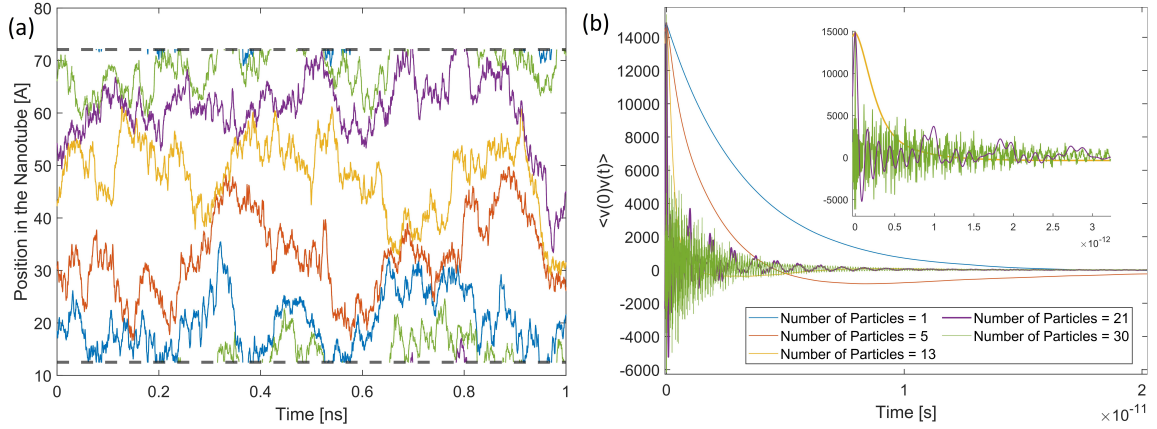


Figure 3.8: (a) Position vs time 5 Particles, calculated with 1D Langevin at  $T=100K$ ,  $\gamma = 0.1$  THz, 1ns. (b) Velocity autocorrelation function for multiple number of particles in 1D Langevin

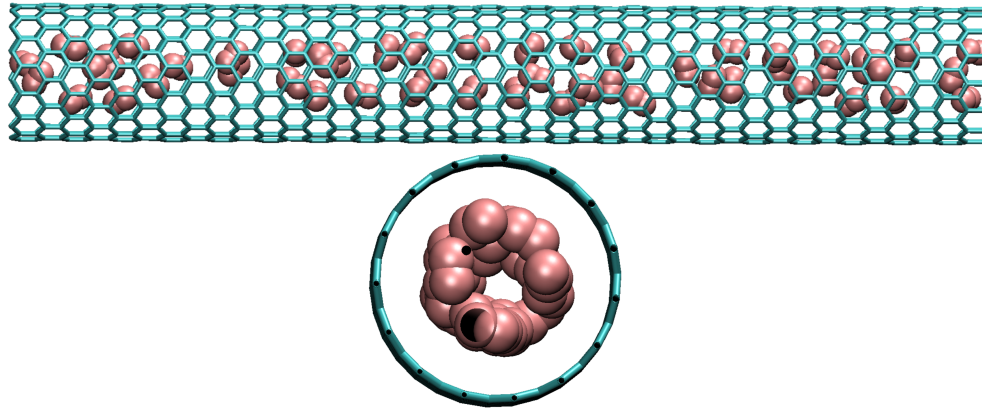


Figure 3.9: Axial and radial spatial distribution of 50 nitrogen molecules inside the swcnt (15,0) at 100K calculated with LAMMPS and represented graphically with VMD (Humphrey et al., 1996)

18.49K for 1D Langevin simulation. This activation energy value would correspond to the height of the potential of the nanotube, whose value is 17.4K (Fig.3.5b). So we find a relative error of 6.26% for LAMMPS and 2.13% for 1D Langevin. These errors are mainly due to the lack of points and statistics of each simulation. This error allows us to check the program used, since it alternatively predicts the value of the potential.

### 3.4 DENSITY-DEPENDENT DIFFUSION

When considering multi-molecule nitrogen systems, we have to implement the new interactions that they generate between them and their transfer of momentum when they collide with each other, these new considerations are detailed in the Section 2.1.2.

In the graphic representation carried out in VMD (Humphrey et al., 1996), we observe

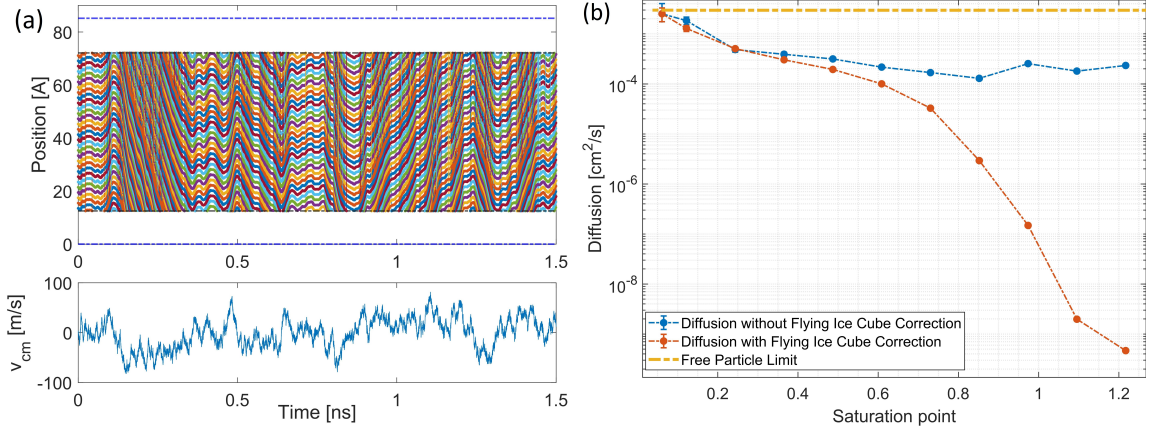


Figure 3.10: (a) Positions vs time 30 nitrogen molecules within SWCNT (15,0) obtained with 1D Langevin.(b) Velocity Vs Time of the center of mass of the 30 nitrogen molecules. (c) Importance of considering the ice cube effect at 100K,  $\gamma = 0.1$  THz, 1D Langevin Blue: Diffusion and number of particles omitting Flying ice cube Effect correction Red: Diffusion vs number of particles considering the Flying ice cube Effect correction

how the nitrogen molecules are distributed uniformly along the axial axis, and in a ring shape on the radial axis, this last behavior was expected by observing the behavior of the axial potential shown in the Fig.3.3c. In the Fig.3.8a we see the positions vs time of 5 nitrogen molecules calculated with 1D Langevin, you can see how the periodic boundary conditions work, the behavior of the random kicks and the collisions between them.

In order to ensure correct obtaining of the diffusion, in each monitoring simulation the convergence of the autocorrelation, as shown in the Fig. 3.8b. The Fig. 3.8b shows that the characteristic decay time is less than  $10\text{ps}$  (which matches the  $\gamma$  value given as input). As another observation, it can be seen that when considering a greater quantity of particles in the system, the decay time of the autocorrelation also decreases considerably. Therefore, times on the order of nanoseconds are more than enough to guarantee a correct diffusion value.

Once the speed and displacement data of the programs used have been obtained, in order to calculate a correct value of the diffusion we must correct the effect of the flying ice cube mentioned in the Section 2.1.3. The graphs shown in Fig. 3.10a allow to understand the artificial effect of the movement of all the particles in a privileged direction.

The Fig. 3.10b diffusion vs number of particles shows how relevant is the influence of considering the flying ice cube effect. The blue curve is the direct calculation of diffusion omitting the correction of the cube effect, where a little monotonic behavior is observed and without a clear trend. On the other hand, the red curve is the diffusion considering the correction of the ice cube, where a monotonic behavior and a clearer trend can be observed.

In order to adequately compare the diffusions found with 1D Langevin and molecular dynamics (LAMMPS) at different amounts of nitrogen molecules, we assume that a valid method

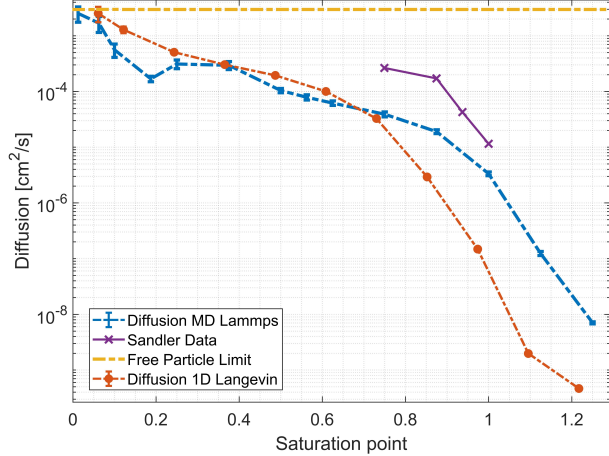


Figure 3.11: Diffusion Vs saturation point. Blue: MD LAMMPS, Red: 1D Langevin, Purple: Data reported by Sandler and Yellow: Free particle limit

is to make dependence of the diffusions with the saturation point of each system. That is, in the case of MD, as reported by Arora et al. (2004), Fig.2.2c, we see that at a concentration of 2 molecules per unit cell, the system is already saturated. In 1D Langevin, we define that the system will be saturated when the number of molecules considered ( $N_{P_{sat}}$ ) in the simulation is equal to the quotient between the diameter of the nitrogen molecules ( $\sigma_{N_2}$ ) and the length of the simulated nanotube ( $L$ ), In other words  $\frac{\sigma_{N_2}}{L} = N_{P_{sat}}$

From the Fig.3.11 we can see that the diffusion calculated with 1D Langevin has a monotonic behavior, decaying relatively slowly until about 0.7 of the saturation point, where the diffusion starts to decline abruptly. The Diffusion found by LAMMPS has characteristics similar to that found with 1D Langevin, where difference is found at low concentrations and at high concentrations. At low concentrations, the diffusion found by LAMMPS does not appear to be monotonic, with a local minimum located near 0.2 of the saturation point, this behavior may be due to two possible reasons: part of the energy of the particle is concentrated in rotating azimuthally. Instead of moving along the axial axis, the other possible reason is the lack of statistics for these data. At high concentrations, above 0.7 of the saturation point, we see a considerable difference where the diffusion of LAMMPS is much greater than that of 1D Langevin, this difference found may be due to the effect that was discussed in the previous section, where the nanotube to having large concentrations of particles (and pressure) nitrogen molecules can now be located in the center of the nanotube allowing a greater cross section of movement and diffusion. The diffusions found in LAMMPS and 1D Langevin at low concentrations or below 0.6 of the saturation point are within the same order of magnitude. Both curves start from the common point of the single molecule. None of the calculated diffusions coincide with data reported by Arora et al. (2004) by at least an order of magnitude.

### 3.5 FUTURE WORK

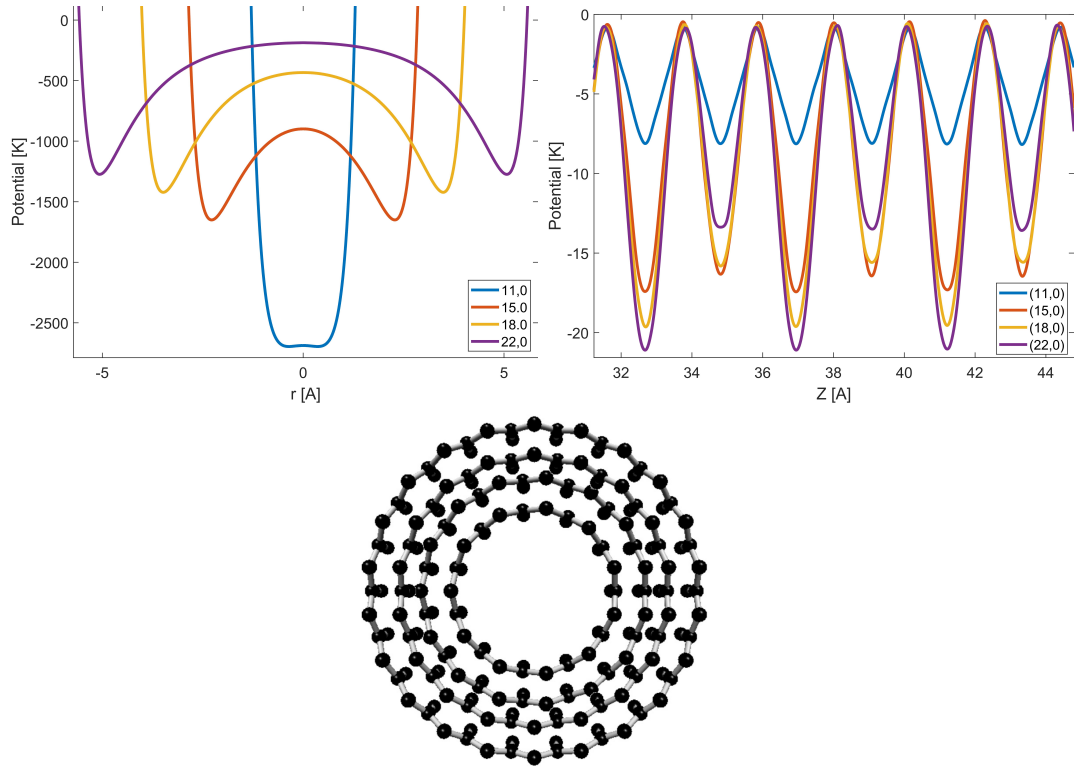


Figure 3.12: Characteristics of Nanotubes of different radius  $8.6\text{\AA}$  (22,0),  $7.1\text{\AA}$  (18,0),  $5.87\text{\AA}$  (15,0),  $4.3\text{\AA}$  (11,0). (a) Radial potential in Kelvin, (b) Axial potential in Kelvin, (c) representation of the radius of the Nanotubes.

As an outlook for future work, it would be interesting to study the effect of the radius of the nanotube on diffusion. As a reference to Fig.3.12a, which shows the radial potential of different nanotubes of different radius, we can expect that using a nanotube (11,0) or smaller radius, the data we obtained using 1D Langevin should match better with 3D MD Simulations, even at high densities or temperatures. This is due to the fact that the radial potential of the nanotube (11,0) is sufficiently narrow preventing the nitrogen molecules from being able to jump over others along the axial axis, resembling more to the conditions imposed in the 1D Langevin simulation. As Fig.3.12b shows we see that the axial potentials of nanotubes of nanotube destinations. For nanotubes with radius greater than (15,0) it does not undergo large changes, only observing a small increase as a function of the increase in radius (from 17 to 22K). On the other hand, with small radius like (11,0) we see that the axial potential decreases considerably (7K), this effect would only be considerable at low temperatures. When considering nanotubes of larger dimensions, the cross section where the nitrogen molecule is capable of moving also increases (Fig.3.12c), increasing the final effective

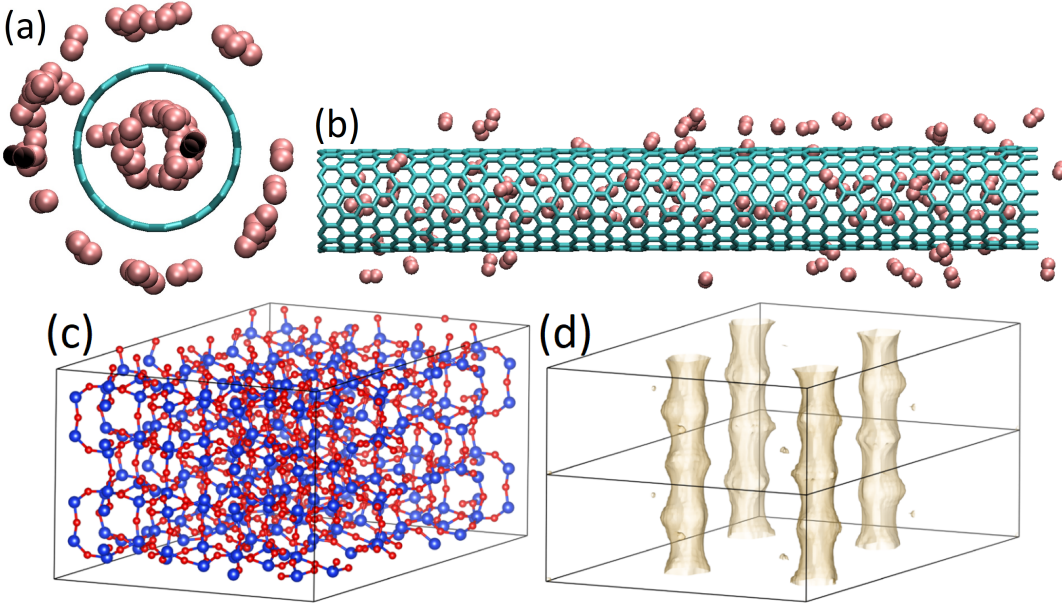


Figure 3.13: (a) and (b) State of a Nanotube after 5ns in a medium in the presence of nitrogen molecules. (c) A  $2 \times 1 \times 1$  supercell of the IZA structure framework of Psi (blue = Si and red = O atoms). (d) The isosurface of the potential energy, adapted from Mace et al. (2019)

diffusion. As mentioned in Sec.2.1.2 The 1D Langevin simulation, the only thing that considers the simulated nanotube is the axial potential As an input parameter, then, if nanotubes of different radii have a similar axial potential, 1D Langevin is unable to distinguish the radial proportions of the nanotube.

Another interesting point to study is how it could use nanotubes as a source of gas storage, and as an external factor (such as a laser) it would be able to extract the stored gases due to an increase in diffusivity in the medium. Fig.3.13 shows the state of a nanotube after 5ns in a medium in the presence of nitrogen molecules, where initially the nanotube was empty. A possible next study is to check how much physics it is possible to recreate in more complex porous media. In Fig.3.13c We observe a more complex porous material where its pores have a geometry similar to nanotubes Fig.3.13d (Mace et al., 2019).

## CHAPTER 4. CONCLUSIONS

One consequence of assuming a diatomic molecule as a solid sphere is to find new parameters of effective potentials that are capable of reproducing the physics that associates the effects of temperature and possible spatial orientations between diatomic molecules. Effective potentials were found between the  $C - N_2$  and  $N_2 - N_2$  interactions, and with these the LJ parameters that reproduce these interactions were determined. Two-dimensional, radial and axial potentials of the nanotube were found, where it was found that the azimuthal potential is not relevant for axial diffusion. In addition, it was found that the radial potential has two very relevant minimums which are the privileged positions where the nitrogen molecules are able to diffuse. The axial potential found has an approximate depth of 17K and resembles a periodic function as a consequence of the periodic geometry of the nanotube.

Using the LAMMPS molecular dynamics program, the diffusion of a molecule at different temperatures within the carbon nanotube was obtained. In this way, a  $\gamma$  parameter was searched in such a way that the data coincided. The  $\gamma$  parameter that satisfies the data obtained with LAMMPS corresponds to the value of 0.1 THz. The differences between LAMMPS and 1D Langevin at low temperatures are due to the calculation of the  $C - N_2$  interaction potential, and at high temperatures it is due to the lack of ability to capture the geometry of the simulated nanotube.

It was possible to calculate and compare the diffusions found from the LAMMPS and 1D Langevin data, finding subtle differences at low concentrations of nitrogen molecules (no more than an order of magnitude), but large differences at high concentrations, this due to the three-dimensional nature considered in LAMMPS that the 1D Langevin algorithm does not contemplate.

## BIBLIOGRAPHY

- Aqel, A., Abou El-Nour, K. M., Ammar, R. A., & Al-Warthan, A. (2012). Carbon nanotubes, science and technology part (i) structure, synthesis and characterisation. *Arabian Journal of Chemistry*, 5(1), 1–23.
- Arora, G., & Sandler, S. I. (2006). Air separation by single wall carbon nanotubes: Mass transport and kinetic selectivity. *The Journal of chemical physics*, 124(8), 084702.
- Arora, G., Wagner, N. J., & Sandler, S. I. (2004). Adsorption and diffusion of molecular nitrogen in single wall carbon nanotubes. *Langmuir*, 20(15), 6268–6277.
- Atomic, L.-s., & Simulator, M. M. P. (2013). Lammps. available at: <http://lammps.sandia.gov>.
- Babaa, M., Stepanek, I., Masenelli-Varlot, K., Dupont-Pavlovsky, N., McRae, E., & Bernier, P. (2003). Opening of single-walled carbon nanotubes: evidence given by krypton and xenon adsorption. *Surface science*, 531(1), 86–92.
- Bojan, M. J., & Steele, W. A. (1987). Interactions of diatomic molecules with graphite. *Langmuir*, 3(6), 1123–1127.
- Braun, E., Moosavi, S. M., & Smit, B. (2018). Anomalous effects of velocity rescaling algorithms: the flying ice cube effect revisited. *Journal of chemical theory and computation*, 14(10), 5262–5272.
- Bukowski, B. C., Keil, F. J., Ravikovitch, P. I., Sastre, G., Snurr, R. Q., & Coppens, M.-O. (2021). Connecting theory and simulation with experiment for the study of diffusion in nanoporous solids. *Adsorption*, (pp. 1–78).
- Cheng, H., Pez, G. P., & Cooper, A. C. (2001). Mechanism of hydrogen sorption in single-walled carbon nanotubes. *Journal of the American Chemical Society*, 123(24), 5845–5846.
- Cundy, C. S., & Cox, P. A. (2005). The hydrothermal synthesis of zeolites: Precursors, intermediates and reaction mechanism. *Microporous and mesoporous materials*, 82(1-2), 1–78.
- Dai, H. (2002). Carbon nanotubes: synthesis, integration, and properties. *Accounts of chemical research*, 35(12), 1035–1044.
- Ganji, M. D., Dalirandeh, Z., & Khorasani, M. (2016). Lithium absorption on single-walled boron nitride, aluminum nitride, silicon carbide and carbon nanotubes: A first-principles study. *Journal of Physics and Chemistry of Solids*, 90, 27–34.

- Goga, N., Rzepiela, A., De Vries, A., Marrink, S., & Berendsen, H. (2012). Efficient algorithms for langevin and dpd dynamics. *Journal of chemical theory and computation*, 8(10), 3637–3649.
- Humphrey, W., Dalke, A., & Schulten, K. (1996). Vmd: visual molecular dynamics. *Journal of molecular graphics*, 14(1), 33–38.
- Khataee, A., Bayat, G., & Azamat, J. (2017). Separation of cyanide from an aqueous solution using armchair silicon carbide nanotubes: insights from molecular dynamics simulations. *RSC advances*, 7(13), 7502–7508.
- Li, C., Meckler, S. M., Smith, Z. P., Bachman, J. E., Maserati, L., Long, J. R., & Helms, B. A. (2018). Engineered transport in microporous materials and membranes for clean energy technologies. *Advanced materials*, 30(8), 1704953.
- Mace, A., Barthel, S., & Smit, B. (2019). Automated multiscale approach to predict self-diffusion from a potential energy field. *Journal of chemical theory and computation*, 15(4), 2127–2141.
- Mirzaei, M., & Mirzaei, M. (2011a). A computational study of aluminum phosphide nanotubes. *International Journal of Quantum Chemistry*, 111(14), 3851–3855.
- Mirzaei, M., & Mirzaei, M. (2011b). A computational study of gallium phosphide nanotubes. *Physica E: Low-dimensional Systems and Nanostructures*, 43(7), 1343–1345.
- Monthioux, M., & Kuznetsov, V. L. (2006). Who should be given the credit for the discovery of carbon nanotubes? *Carbon*, 44(9), 1621–1623.
- Moon, W. C. (2019). A review on interesting properties of chicken feather as low-cost adsorbent. *International Journal of Integrated Engineering*, 11(2).
- Nanotube-Modeler (2004-2005). Jcrystalsoft, 2004–2005.
- Nicholson, D. (2002). A simulation study of the pore size dependence of transport selectivity in cylindrical pores. *Molecular Physics*, 100(13), 2151–2163.
- Noei, M., Soleymanabadi, H., & Peyghan, A. A. (2017). Aluminum nitride nanotubes. *Chemical Papers*, 71(5), 881–893.
- Pederson, M. R., & Broughton, J. Q. (1992). Nanocapillarity in fullerene tubules. *Physical Review Letters*, 69(18), 2689.
- Rouhi, S. (2016). Molecular dynamics simulation of the adsorption of polymer chains on cnts, bnnts and gannts. *Fibers and Polymers*, 17(3), 333–342.
- Saufi, S., & Ismail, A. (2004). Fabrication of carbon membranes for gas separation—a review. *Carbon*, 42(2), 241–259.

- Sokhan, V., Nicholson, D., & Quirke, N. (2004). Transport properties of nitrogen in single walled carbon nanotubes. *The Journal of chemical physics*, 120(8), 3855–3863.
- Stock, N., & Biswas, S. (2012). Synthesis of metal-organic frameworks (mofs): routes to various mof topologies, morphologies, and composites. *Chemical reviews*, 112(2), 933–969.
- Travis, K. P., & Gubbins, K. E. (1999). Transport diffusion of oxygen- nitrogen mixtures in graphite pores: A nonequilibrium molecular dynamics (nemd) study. *Langmuir*, 15(18), 6050–6059.
- Tsang, S., Chen, Y., Harris, P., & Green, M. (1994). A simple chemical method of opening and filling carbon nanotubes. *Nature*, 372(6502), 159–162.
- Wang, Q., Challa, S. R., Sholl, D. S., & Johnson, J. K. (1999). Quantum sieving in carbon nanotubes and zeolites. *Physical Review Letters*, 82(5), 956.
- Wang, X. L., Han, X., & Yu, S. J. (2013). Synthesis and application of porous nanomaterials. In *Advanced Materials Research*, vol. 788, (pp. 7–10). Trans Tech Publ.
- Williams, K. A., Veenhuizen, P. T., Beatriz, G., Eritja, R., & Dekker, C. (2002). Carbon nanotubes with dna recognition. *Nature*, 420(6917), 761–761.
- Zhu, Z., Wei, N., Cheng, W., Shen, B., Sun, S., Gao, J., Wen, Q., Zhang, R., Xu, J., Wang, Y., et al. (2019). Rate-selected growth of ultrapure semiconducting carbon nanotube arrays. *Nature communications*, 10(1), 1–8.
- Zwanzig, R. (2001). *Nonequilibrium statistical mechanics*. Oxford University Press.

## APPENDIX A. DESCRIPTION OF THE MATLAB LANGEVIN PROGRAM

The program used can be summarized with the following sections, of which we will describe in more detail in Figure A.1. The first section of the program initially introduces all the universal constants that are considered in the program, such as Boltzmann's constant [J/K], charge of the electron [C] and the atomic mass unit [kg]. Later are the relevant parameters of the simulation (Temperature, mass of the molecule,  $\gamma$ , time step, total time) and of the nanotube (chirality). The last part of this section is to load the nanotube coordinate file (xyz file).

The second section takes the nanotube coordinate file, and calculates the radial potential at different points of the nanotube using the equation (with the effective parameters found in the previous section), concluding in an effective radial potential (obtaining the potential shown in). Once this effective potential is obtained, we find the most probable radial position where the nitrogen molecule would be. Then we calculate the axial potential, which will be the one that will be worked on.

The third section begins with a "for" loop that sets the number of molecules that the nanotube will contain.

Within this for loop, there is another for loop that sets the number of independent systems " $N_s$ " (keeping all the parameters) will be simulated, in order to have better statistics.

We make use of a previously made script, where the input is all the files, parameters and potential previously calculated and its ouput the diffusion of the  $N_p$  particles in vector form. The aforementioned script performs the dynamics of the  $N_p$  particles using the Langevin algorithm. Obtaining the speed and position of each particle, at this point a speed correction is made by the frying ice cube mentioned in the section. It is worth mentioning that a thermalization process of 0.5ns is carried out. Then the autocorrelation of the speed of each  $N_p$  molecule is carried out, obtaining the  $N_p$  diffusions mentioned in the previous paragraph.

At the end of this second for loop, we obtain a diffusion vector of  $N_p \cdot N_s$  particles. Then using these diffusion data, we obtain the probability density function from which we obtain the effective diffusion with its corresponding error for a given number of nitrogen molecules.

Finally finished the first cycle for, already simulated all the systems with different numbers of particles, we obtain a vector of diffusion in function of molecules inside the nanotube " $D(N_p)$ ".

60 runs were performed for each quantity of particle established.

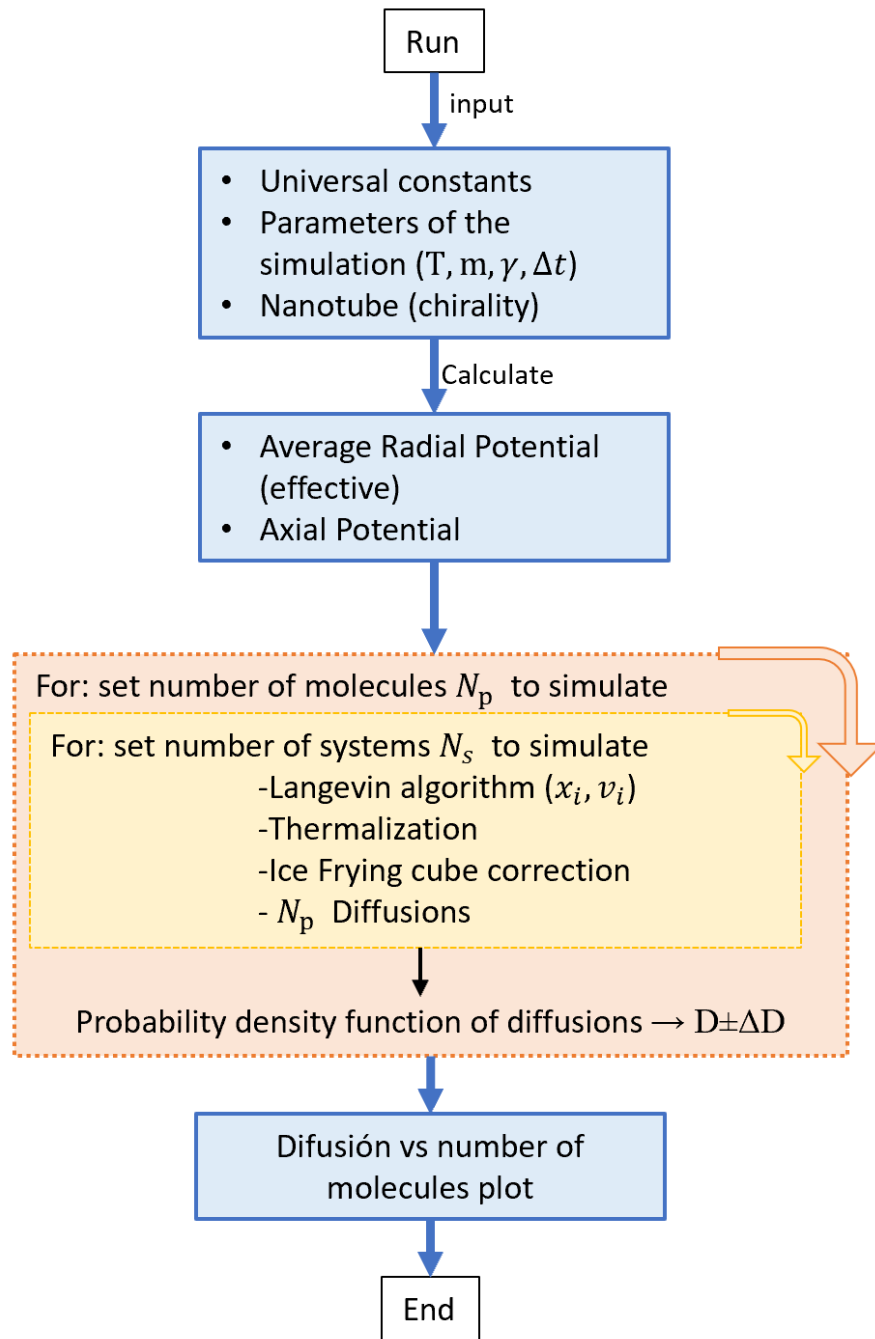


Figure A.1: Flow Chart of the MATLAB program used.

## APPENDIX B. LAMMPS INPUT SCRIPT

10 runs were performed for the single particle and one run for higher densities, this due to the computational load needed.

```
units real
dimension 3
boundary p p p
atom_style full
pair_style lj/cut 8.52
variable T equal 100.0
box tilt large
read_data Nanotube_15fix100p.data
pair_coeff 1 2 0.06677 3.36 8.52
pair_coeff 1 1 0.072334 3.32 8.3
pair_coeff 2 2 0 0
neighbor 2.0 bin
neigh_modify check yes
group carbon type 2
group nitro type 1
timestep 1
run_style verlet
compute 3 nitro msd
thermo_style custom step dt temp pe c_3[3] c_3[4]
thermo 10000
thermo_modify flush yes
compute 1 all pe
fix NVT nitro rigid/nvt molecule temp T 100.0
run 50000
unfix NVT
reset_timestep 0
fix NVT nitro rigid/nvt molecule temp TT 100.0
dump 1 nitro custom 100 nitroNpTk_n.dump id mol type x y z vx vy vz xu yu zu iz
dump_modify 1 flush yes
run 5000000
write_restart restart_nitro_production
```